53. Emilie D, Peuchmaur M, Maillot MC, Crevon MC, Brousse N, et al. (1990) Production of interleukins in human immunodeficiency virus-1-replicating lymph nodes. J Clin Invest 86: 148–159.
54. Brenchley JM, Price DA, Schacker TW, Asher TE, Silvestri G, et al. (2006) Microbial translocation is a cause of systemic immune activation in chronic HIV infection. Nat Med 12: 1365–1371.
55. Akira S, Takeda K, Kaisho T (2001) Toll-like receptors: critical proteins linking innate and acquired immunity. Nat Immunol 2: 675–680.
56. Sauter B, Albert ML, Francisco L, Larsson M, Somersan S, et al. (2000) Consequences of cell death: exposure to necrotic tumor cells, but not primary tissue cells or apoptotic cells, induces the maturation of immunostimulatory dendritic cells. J Exp Med 191: 423–434.
57. Basu S, Binder RJ, Suto R, Anderson KM, Srivastava PK (2000) Necrotic but not apoptotic cell death releases heat shock proteins, which deliver a partial maturation signal to dendritic cells and activate the NF-κB pathway. Int Immunol 12: 1539–1546.
58. Ostrand-Rosenberg S, Sinha P, Beury DW, Clements VK (2012) Cross-talk between myeloid-derived suppressor cells (MDSC), macrophages, and dendritic cells enhances tumor-induced immune suppression. Semin Cancer Biol 22: 275–281.
59. Gabrilovich DI, Nagaraj S (2009) Myeloid-derived suppressor cells as regulators of the immune system. Nat Rev Immunol 9: 162–174.
60. Gorantla S, Makarov E, Finke-Dwyer J, Gebhart CL, Domm W, et al. (2010) $CD8^+$ cell depletion accelerates HIV-1 immunopathology in humanized mice. J Immunol 184: 7082–7091.
61. Baenziger S, Tussiwand R, Schlaepfer E, Mazzucchelli L, Heikenwalder M, et al. (2006) Disseminated and sustained HIV infection in $CD34^+$ cord blood cell-transplanted $Rag2^{-/-}\gamma_c^{-/-}$ mice. Proc Natl Acad Sci U S A 103: 15951–15956.
62. Watanabe S, Ohta S, Yajima M, Terashima K, Ito M, et al. (2007) Humanized NOD/SCID/IL2Rγ^{null} mice transplanted with hematopoietic stem cells under nonmyeloablative conditions show prolonged life spans and allow detailed analysis of human immunodeficiency virus type 1 pathogenesis. J Virol 81: 13259–13264.
63. Watanabe S, Terashima K, Ohta S, Horibata S, Yajima M, et al. (2007) Hematopoietic stem cell-engrafted NOD/SCID/IL2Rγ^{null} mice develop human lymphoid systems and induce long-lasting HIV-1 infection with specific humoral immune responses. Blood 109: 212–218.
64. Sato K, Koyanagi Y (2011) The mouse is out of the bag: insights and perspectives on HIV-1-infected humanized mouse models. Exp Biol Med (Maywood) 236: 977–985.
65. Berges BK, Rowan MR (2011) The utility of the new generation of humanized mice to study HIV-1 infection: transmission, prevention, pathogenesis, and treatment. Retrovirology 8: 65.
66. Shultz LD, Brehm MA, Garcia-Martinez JV, Greiner DL (2012) Humanized mice for immune system investigation: progress, promise and challenges. Nat Rev Immunol 12: 786–798.
67. Levy DN, Refaeli Y, MacGregor RR, Weiner DB (1994) Serum Vpr regulates productive infection and latency of human immunodeficiency virus type 1. Proc Natl Acad Sci U S A 91: 10873–10877.
68. Hoshino S, Sun B, Konishi M, Shimura M, Segawa T, et al. (2007) Vpr in plasma of HIV type 1-positive patients is correlated with the HIV type 1 RNA titers. AIDS Res Hum Retroviruses 23: 391–397.
69. Zimmerman ES, Sherman MP, Blackett JL, Neidleman JA, Kreis C, et al. (2006) Human immunodeficiency virus type 1 Vpr induces DNA replication stress *in vitro* and *in vivo*. J Virol 80: 10407–10418.
70. Sakai K, Dimas J, Lenardo MJ (2006) The Vif and Vpr accessory proteins independently cause HIV-1-induced T cell cytopathicity and cell cycle arrest. Proc Natl Acad Sci U S A 103: 3369–3374.
71. Wang J, Shackelford JM, Casella CR, Shivers DK, Rapaport EL, et al. (2007) The Vif accessory protein alters the cell cycle of human immunodeficiency virus type 1 infected cells. Virology 359: 243–252.
72. Izumi T, Io K, Matsui M, Shirakawa K, Shinohara M, et al. (2010) HIV-1 viral infectivity factor interacts with TP53 to induce G2 cell cycle arrest and positively regulate viral replication. Proc Natl Acad Sci U S A 107: 20798–20803.
73. Ito M, Hiramatsu H, Kobayashi K, Suzue K, Kawahata M, et al. (2002) NOD/SCID/γ_c^{null} mouse: an excellent recipient mouse model for engraftment of human cells. Blood 100: 3175–3182.
74. An DS, Poon B, Ho Tsong Fang R, Weijer K, Blom B, et al. (2007) Use of a novel chimeric mouse model with a functionally active human immune system to study human immunodeficiency virus type 1 infection. Clin Vaccine Immunol 14: 391–396.

Published August 26, 2013, doi:10.4049/jimmunol.1203543

Establishment of a Human Allergy Model Using Human IL-3/GM-CSF–Transgenic NOG Mice

Ryoji Ito,*,† Takeshi Takahashi,* Ikumi Katano,* Kenji Kawai,* Tsutomu Kamisako,* Tomoyuki Ogura,* Miyuki Ida-Tanaka,* Hiroshi Suemizu,* Satoshi Nunomura,‡ Chisei Ra,‡ Akio Mori,§ Sadakazu Aiso,† and Mamoru Ito*

The development of animal models that mimic human allergic responses is crucial to study the pathophysiology of disease and to generate new therapeutic methodologies. Humanized mice reconstituted with human immune systems are essential to study human immune reactions in vivo and are expected to be useful for studying human allergies. However, application of this technology to the study of human allergies has been limited, largely because of the poor development of human myeloid cells, especially granulocytes and mast cells, which are responsible for mediating allergic diseases, in conventional humanized mice. In this study, we developed a novel transgenic (Tg) strain, NOD/Shi-*scid*-IL2rγ^{null} (NOG), bearing human *IL-3* and *GM-CSF* genes (NOG IL-3/GM–Tg). In this strain, a large number of human myeloid cells of various lineages developed after transplantation of human CD34$^+$ hematopoietic stem cells. Notably, mature basophils and mast cells expressing FcεRI were markedly increased. These humanized NOG IL-3/GM–Tg mice developed passive cutaneous anaphylaxis reactions when administered anti–4-hydroxy-3-nitrophenylacetyl IgE Abs and 4-hydroxy-3-nitrophenylacetyl. More importantly, a combination of serum from Japanese cedar pollinosis patients and cedar pollen extract also elicited strong passive cutaneous anaphylaxis responses in mice. Thus, to our knowledge, our NOG IL-3/GM–Tg mice are the first humanized mouse model to enable the study of human allergic responses in vivo and are excellent tools for preclinical studies of allergic diseases. *The Journal of Immunology*, **2013, 191: 000–000.**

Rodent models for human allergies, including atopic dermatitis (1), asthma (2), allergic rhinitis (3), and food allergies (4, 5), have allowed researchers to elucidate important fundamental principles of the cellular and molecular mechanisms of these diseases. However, it was suggested that animal models do not always reflect all aspects of human allergic diseases because of differences between species. The gap between these animal models and human clinical settings has prevented the development of effective therapeutic strategies for the treatment of human allergies.

Reconstitution of human hematopoietic and immune systems in immunodeficient mouse strains was a major advance in the field of humanized mouse technologies within the last 2 decades. These mouse models were expected to recapitulate various human diseases, including cancer (6–9), infectious disease (10–14), and graft-versus-host-disease (GVHD) (15, 16), and to enhance basic research in human physiology and pathology, as well as the development of clinical drugs. Recently, severely immunodeficient mouse strains, such as NOD/Shi-*scid* IL2rγ^{null} (NOG) (17–19), NOD/LtSz-*scid* IL2rγ^{null} (NSG) (20), and BALB/c Rag2^{null} IL2rγ^{null} (21, 22), enabled long-term engraftment of human tissues because of the total lack of the endogenous mouse immune system, enormously improving the generation of humanized mice. Our group previously demonstrated that efficient human hematopoiesis could be seen in NOG mice upon transplantation of human hematopoietic stem cells (HSCs; hu-HSC NOG mice) (17, 23). In particular, lymphopoiesis was evident, and human B and T cells accounted for the majority of human cells in hu-HSC NOG mice. Accumulating evidence suggests that these human lymphocytes can mediate proper immune reactions, even if the response remains suboptimal. In contrast, the differentiation of human myeloid lineage cells, especially granulocytes and mast cells, in conventional hu-HSC NOG mice has been inefficient (23, 24). Considering the emerging roles of granulocytes and mast cells in allergic inflammatory diseases, it is important to establish useful animal models in which we can analyze and manipulate the functions of human granulocytes and mast cells. Poor differentiation of these cells may be attributed, in part, to an insufficient supply of cytokines, such as G-CSF, GM-CSF, IL-3, IL-6, Fms-related tyrosine kinase 3 ligand, thrombopoietin (TPO), and stem cell factor (SCF) (25–29). Recently, several groups attempted to improve the efficiency of human granulopoiesis in humanized mice by engineering mice to express human genes encoding these cytokines. Billerbeck et al. (30) developed a transgenic (Tg) NSG mouse strain expressing human (h) SCF, hGM-CSF, and hIL-3 (SGM3-Tg) and demonstrated that the development of CD33$^+$ myeloid cells and CD15$^+$ granulocytes was

*Central Institute for Experimental Animals, Kawasaki-ku, Kawasaki, Kanagawa 210-0821, Japan; †Department of Anatomy, Keio University School of Medicine, Shinjuku-ku, Tokyo 160-8582, Japan; ‡Division of Molecular Cell Immunology and Allergology, Nihon University, Graduate School of Medical Science, Itabashi-ku, Tokyo 173-8610, Japan; and §National Hospital Organization, Sagamihara National Hospital, Clinical Research Center, Minami-ku, Sagamihara, Kanagawa 252-0315, Japan

Received for publication December 27, 2012. Accepted for publication July 16, 2013.

This work was supported by a grant from the Research Foundation for Pharmaceutical Sciences and by Grants-in-Aid for Young Scientists (B) 22700458 and Scientific Research (S) 22220007 from the Ministry of Education, Culture, Sports, Science and Technology of Japan.

Address correspondence and reprint requests to Dr. Mamoru Ito, Central Institute for Experimental Animals, 3-25-12 Tonomachi, Kawasaki-ku, Kawasaki, Kanagawa 210-0821, Japan. E-mail address: mito@ciea.or.jp

The online version of this article contains supplemental material.

Abbreviations used in this article: BALF, bronchoalveolar lavage fluid; BM, bone marrow; CIEA, Central Institute for Experimental Animals; GVHD, graft-versus-host disease; h, human; HSC, hematopoietic stem cell; KI, knock-in; m, mouse; MCC, mast cell chymase; MCT, mast cell containing tryptase; MCTC, mast cell containing tryptase and chymase; NOG, NOD/Shi-*scid* IL2rγ^{null}; NP, 4-hydroxy-3-nitrophenylacetyl; NSG, NOD/LtSz-*scid* IL2rγ^{null}; PB, peripheral blood; PCA, passive cutaneous anaphylaxis; SCF, stem cell factor; Tg, transgenic; TPO, thrombopoietin.

www.jimmunol.org/cgi/doi/10.4049/jimmunol.1203543

slightly enhanced in SGM3-Tg mice compared with non-Tg control mice following transplantation with hHSCs. Furthermore, Rongvaux et al. (31) established hTPO knock-in (KI) mice in which the mouse *TPO* gene locus was replaced with the corresponding human gene locus. Upon transplantation of hHSCs, this strain showed remarkable differentiation of monocytes and granulocytes. However, generation of mast cells and several granulocyte subpopulations remained insufficient. Moreover, although the efficient development of human granulocytes and mast cells was demonstrated in humanized membrane-bound SCF-Tg NSG mice (32), the function of granulocytes in humanized SCF-Tg NSG mice has not been verified, especially with respect to whether they could release cytoplasmic granules containing histamine, leukotriene, and so forth in response to stimulation.

In this study, we generated a novel NOG substrain: hIL-3 and hGM-CSF–Tg (IL-3/GM–Tg) NOG mice. Within this model, we studied the development of human myeloid cells, maturation of basophils and mast cells, and passive cutaneous anaphylaxis (PCA) reaction in response to Ag-specific hIgE and the specific Ags. Our results effectively support the usefulness of this novel platform for studying human allergies.

Materials and Methods

Ethics statement

All animal experiments were approved by the Institutional Animal Care and Use Committee of the Central Institute for Experimental Animals (CIEA) and were performed in accordance with guidelines set forth by the CIEA.

All experiments using human cells and serum were approved by the institutional ethical committee of the CIEA and Sagamihara National Hospital. Written informed consent was obtained from every subject enrolled in the current study.

Generation of NOG IL-3/GM–Tg mice

Previously, we established a hIL-3 and hGM-CSF Tg C57BL/6J-*scid* mouse strain in which the Tg human genes were ubiquitously expressed under control of the SRα promoter (33). This strain was backcrossed six times with NOG (formal name: NOD.Cg-*prkdc*^{scid}*il2r*γ^{tm1Sug}/ShiJic) mice to replace the genetic background with the aid of a marker-assisted selection protocol. Serum levels of hIL-3 and hGM-CSF were measured using human IL-3 and human GM-CSF Quantikine ELISA Kits (R&D Systems, Minneapolis, MN). The mice were maintained in the CIEA under specific pathogen–free conditions.

Human HSC transplantation

Human umbilical cord blood–derived CD34$^+$ cells were purchased from Lonza (cat. no. 2C-101A; Basel, Switzerland). After thawing the frozen vials of cells according to the manufacturer's protocol, cells with >90% viability were used for transplantation. NOG IL-3/GM–Tg or non-Tg mice (8–10 wk old) were irradiated with x-rays (2.5 Gy; MBR-1505R; Hitachi Medical, Tokyo, Japan). After 24 h, 4–5 × 10^4 hHSCs were transplanted i.v. via the tail vein.

Flow cytometry

Bone marrow (BM), spleen, peripheral blood (PB), and bronchoalveolar lavage fluid (BALF) tissues were obtained from mice transplanted with hHSCs. Single mononuclear cell suspensions were prepared by standard methods, and RBCs were eliminated using BD Pharm Lyse (BD Biosciences, San Jose, CA). Human PB samples were obtained from healthy volunteers after acquiring their informed consent. hPBMCs were isolated by Ficoll-Hypaque (GE Healthcare, Little Chalfont, Buckinghamshire, U.K.) density centrifugation and washed with PBS. The cells were incubated with appropriate fluorochrome-conjugated Abs for 15–20 min at 4°C. After washing with FACS buffer containing PBS with 1% FCS, the cells were resuspended in propidium iodide solution (BD Biosciences). Fluorescent signals were measured using a FACSCanto multicolor flow cytometer, and the data were analyzed using FACSDiva software (both from BD Biosciences). We used the following Abs: anti-hCD33–FITC and anti–mouse (m)CD45–biotin (BD Biosciences); anti-hCD19–PE (Beckman Coulter, Brea, CA); and anti-hCD45–allophycocyanin–Cy7, anti-hCD66b–FITC, anti-hLineage mixture (CD3, CD14, CD19, CD20, CD56)–FITC, anti-hCD56–PE, anti-hCD203c–PE, anti-hCD38–PE, anti-hCD34–PE–Cy7, anti-hCD3–PE–Cy7, anti–hc-kit–PE–Cy7, anti-CD14–PE–Cy7, anti-hFcεRI–allophycocyanin, and anti-hCD11c–allophycocyanin (BioLegend, San Diego, CA).

Determination of human granulocytes

At 11 wk after HSC transplantation, PB was collected from the orbital vein of humanized NOG IL-3/GM–Tg and non-Tg NOG mice under anesthesia. Single-cell suspensions were prepared using BD Pharm Lyse (BD Biosciences), and hCD45$^+$ cells were purified by eliminating mCD45$^+$ cells using MACS. Briefly, the cells were stained with biotinylated anti-mCD45 Abs in MACS running buffer (PBS containing 2 mM EDTA and 0.1% BSA) for 15 min at 4°C. The cells were washed with MACS buffer and subsequently labeled with anti-biotin magnetic beads (Miltenyi Biotec, Sunnyvale, CA). Labeled mCD45$^+$ cells were eliminated using a MACS LS column (Miltenyi Biotec). The purity of hCD45$^+$ cells in the negative fraction was typically 95–99%.

For May–Grünwald–Giemsa staining, enriched hCD45$^+$ cells were smeared onto glass slides and air dried for 10 min. The slides were soaked in May–Grünwald solution (Muto Pure Chemicals, Tokyo, Japan) for 3 min and then washed with running water to remove excess stain. The slides were further stained with 0.5% Giemsa solution (Muto Pure Chemicals) for 15 min. After washing with running water, the slides were dried and subjected to microscopic analyses.

In vitro stimulation of human basophils and mast cells

At 18 wk after HSC transplantation, BM mononuclear cells from NOG IL-3/GM–Tg mice and hPBMCs were stimulated with 1 μg/ml ionomycin (Sigma-Aldrich, St. Louis, MO) for 30 min at 37°C in a 5% CO_2 incubator. After stimulation, these cells were stained with allophycocyanin-Cy7–anti-hCD45, FITC–anti-hCD63 (Beckman Coulter), PE–anti-hCD203, and allophycocyanin–anti-hFcεR mAbs and were analyzed by flow cytometer.

Immunohistochemistry

For histological analyses, the lungs, spleen, stomach, and skin from humanized NOG IL-3/GM–Tg and non-Tg mice were fixed with 4% paraformaldehyde (Wako, Osaka, Japan) and embedded in paraffin. The samples were then serially sectioned to a thickness of 3 μm using a microtome and placed on silane-coated slides (Muto Pure Chemicals). After deparaffinization, sections were incubated overnight at 4°C with anti-human mast cell chymase (MCC) Abs (clone CC1; Leica Microsystems, Tokyo, Japan) and anti-human FcεRI Ab (clone CRA-1) (34, 35) and then incubated with a peroxidase-labeled polymer-conjugated anti-mouse Ab (Histofine Simple Stain Max-PO; Nichirei Biosciences, Tokyo, Japan) for 30 min at room temperature. For color development, the sections were incubated with a 0.02% solution of the substrate 3,3′-diaminobenzidine (Dojindo, Kumamoto, Japan) containing 0.006% H_2O_2. Immunostained sections were counterstained with hematoxylin (Sakura Finetech, Tokyo, Japan) for visualization of nuclei. For immunofluorescence staining, 4-μm-thick frozen sections of tissues were fixed in 99% ethanol for 30 min and incubated with 10% normal goat serum (Nichirei Biosciences) for 30 min. An anti-human mast cell tryptase mAb (clone 10D11; Leica Microsystems) or an anti-human MCC mAb was fluorescently labeled with either Alexa Fluor 488 or Alexa Fluor 546 using a Zenon Mouse IgG2b or IgG1 Kit (Life Technologies, Carlsbad CA), according to the manufacturer's instructions, and we used these mAbs for double staining of the sections. After a 2-h incubation at room temperature, the sections were washed five times with PBS and mounted with ImmunoSelect Antifading Mounting Medium DAPI (Dianova, Hamburg, Germany). The specimens were visualized by fluorescence microscopy (Axio Imager M1; Carl Zeiss Microscopy, Tokyo Japan).

PCA reactions

An anti–4-hydroxy-3-nitrophenylacetyl (NP) human/mouse chimeric IgE Ab (Serotec, Oxford, U.K.), which is composed of murine V region and human C region, was injected intradermally at six locations (0.5 μg/location) on the dorsal side of humanized NOG IL-3/GM–Tg, non-Tg, and nonhumanized NOG mice. The same amount of hIgE Ab (Abcam, Tokyo, Japan) was injected into the ventral side of the mice as negative controls. Twenty-four hours after sensitization, the mice were injected i.v. with 500 μg NP-conjugated BSA (Biosearch Technologies, Novato, CA) with 0.5% Evans blue dye. Extravasation of the dye was visualized 30 min later by observing the blue staining of the reverse-side sites on the opposite side of the injection sites. For pollinosis PCA reaction, Japanese cedar pollinosis patients were recruited from the outpatient clinic of Sagamihara National Hospital. Japanese cedar pollen–specific IgE titer in the serum was determined by CAP-RAST. Serum obtained from Japanese cedar

Table I. Generation of hIL-3/GM-CSF–Tg NOG mice

Generation	NOD Marker (%)	Cytokine Levels in Sera (pg/ml)	
		hIL−3	hGM−CSF
N0	0	ND	ND
N1	50	ND	ND
N2	81	ND	ND
N3	93	106.7 ± 14.7	67.1 ± 27.5
N4	98	ND	ND
N5	98	74.4 ± 44.7	51.4 ± 40.5
N6	100	ND	ND
N7	100	82.04 ± 40.24	35.03 ± 11.6

ND, Not determined.

pollinosis patients (carrier polymer radioallergosorbent score = 5) was diluted 2-fold in saline and injected intradermally at two locations on the dorsal side of the mice. After 24 h, these mice were injected i.v. with 100 μl the cedar pollen extract (200 JAU/ml; Torii Pharmaceutical, Tokyo, Japan) with 0.5% Evans blue dye. After 30 min, dorsal or ventral skins from these mice were isolated and weighed. Evans blue dye was extracted from the skin by incubation in 5 ml formamide at 60°C overnight and quantified by OD at 620 nm in a spectrometer (Bio-Rad, Tokyo, Japan).

Statistical analysis

Mean values and SD were calculated using Microsoft Excel (Microsoft, Redmond, WA). Student *t* tests were used to identify significant differences.

Results

Generation of NOG IL-3/GM–Tg mice

We generated NOG IL-3/GM–Tg mice by speed congenic techniques using a marker-assisted selection protocol (36) to change the genetic background of the mice from C57BL/6J to NOD. IL-3/GM–Tg mice, in which all of the microsatellite markers were replaced by the NOD haplotype at N6, were further crossed onto the NOG background. We confirmed the expression of the hIL-3 and hGM-CSF transgenes in the N3, N5, and N7 generations (Table I). For hHSC transfer, we used NOG IL-3/GM–Tg mice backcrossed more than seven times.

Human hematopoiesis in hu-HSC NOG IL-3/GM–Tg mice

To investigate the effects of hIL-3 and hGM-CSF on hematopoiesis in humanized mice, we transplanted hCD34$^+$ HSCs into NOG IL-3/GM–Tg and non-Tg mice. The frequencies of hCD45$^+$ cells and various lineages of human leukocytes in PB and various tissues

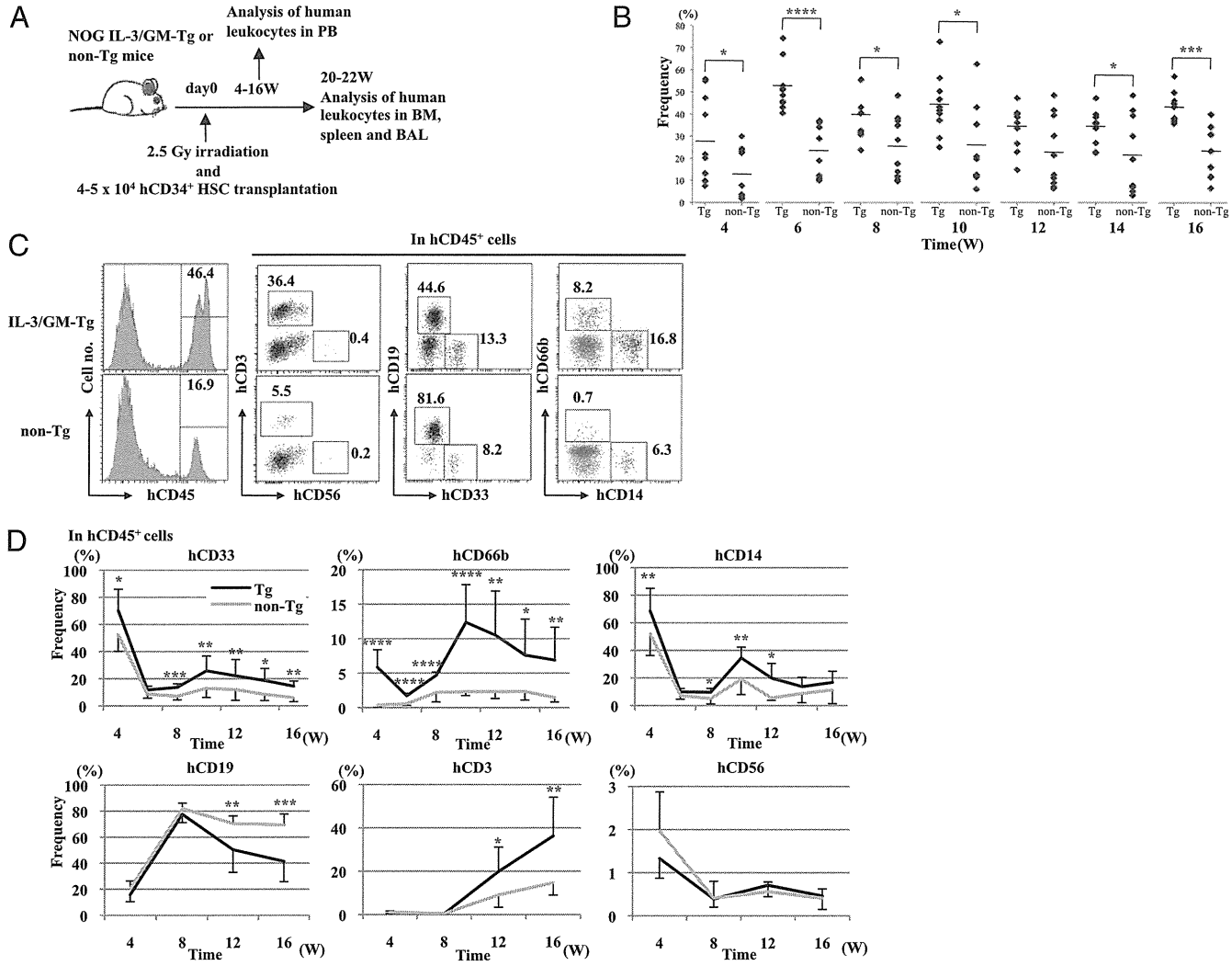

FIGURE 1. Human hematopoiesis in NOG IL-3/GM–Tg mice. (**A**) Schematic view of the reconstitution of human immune systems in NOG IL-3/GM–Tg mice. NOG IL-3/GM–Tg mice and non-Tg littermates (8–10 wk old) were transplanted with 4–5 × 10^4 hCD34$^+$ HSCs 1 d after x-ray irradiation (2.5 Gy). Human leukocytes were analyzed at the indicated time points. (**B**) Kinetics of hCD45$^+$ cell engraftment. The frequency of human leukocytes in PB was analyzed by flow cytometry at the indicated time points over 12 wk. Data are mean ± SD (n = 10 mice/group). (**C** and **D**) Frequencies of engrafted multilineage hCD19$^+$, hCD3$^+$, hCD56$^+$, hCD33$^+$, hCD66b$^+$, and hCD14$^+$ human leukocytes in the hCD45$^+$ cell population were analyzed by flow cytometry. *$p < 0.05$, **$p < 0.005$, ***$p < 0.0005$, ****$p < 0.00005$.

from these mice were analyzed at different time points (Fig. 1A). The chimerism of hCD45$^+$ cells in PB was significantly higher in hu-HSC NOG IL-3/GM–Tg mice than in non-Tg NOG mice throughout the analysis period (Fig. 1B, 1C). For the myeloid lineage, hu-HSC NOG IL-3/GM–Tg mice had significantly higher frequencies of total hCD33$^+$ myeloid cells, hCD66b$^+$ granulocytes, and hCD14$^+$ monocytes than did non-Tg mice (Fig. 1C, 1D). In particular, the increase in hCD66b$^+$ granulocytes was dramatic compared with the low differentiation of this population in conventional NOG mice. For lymphoid cells, the increase in the hCD3$^+$ T cell population was more evident in Tg mice than in non-Tg mice at 12 wk post-HSC transplantation, resulting in a lower frequency of hCD19$^+$ B cells in Tg mice than in non-Tg mice; the development of hCD56$^+$ NK cells was not influenced (Fig. 1C, 1D). Human leukocytes, other than lymphoid and myeloid lineage cells, were scarce in hCD45$^+$ cells in PB of Tg and non-Tg mice (Supplemental Fig. 1A).

We next investigated other organs. The engraftment of human HSCs, defined as hCD34$^+$hCD38$^-$ cells in hCD45$^+$lineage$^-$ cells, in the BM showed 4- and 3-fold increases in frequency and cell number, respectively, in Tg mice compared with non-Tg mice (Fig. 2A, 2B). Spleens were markedly enlarged in hu-HSC NOG IL-3/GM–Tg mice (Supplemental Fig. 1B). Consistent with this finding, weight and total splenocyte numbers were ~3-fold higher in Tg mice than in non-Tg mice (Supplemental Fig. 1C, 1D). Although the percentage of CD45$^+$ cells did not differ between Tg and non-Tg mice, the absolute number of hCD45$^+$ cells increased in Tg mice, reflecting an increase in total cell number (Fig. 2C, 2D). As in the PB, the frequency and absolute number of hCD33$^+$ myeloid cells in the spleen were increased in hu-HSC–Tg mice, and expansion of hCD66b$^+$ granulocytes was especially remarkable (Fig. 2D, 2E). An increase in the hCD33$^+$hCD11c$^+$ myeloid dendritic cell population was also confirmed (Fig. 2D, 2E). In addition, the number of cells in BALF samples was increased 4-

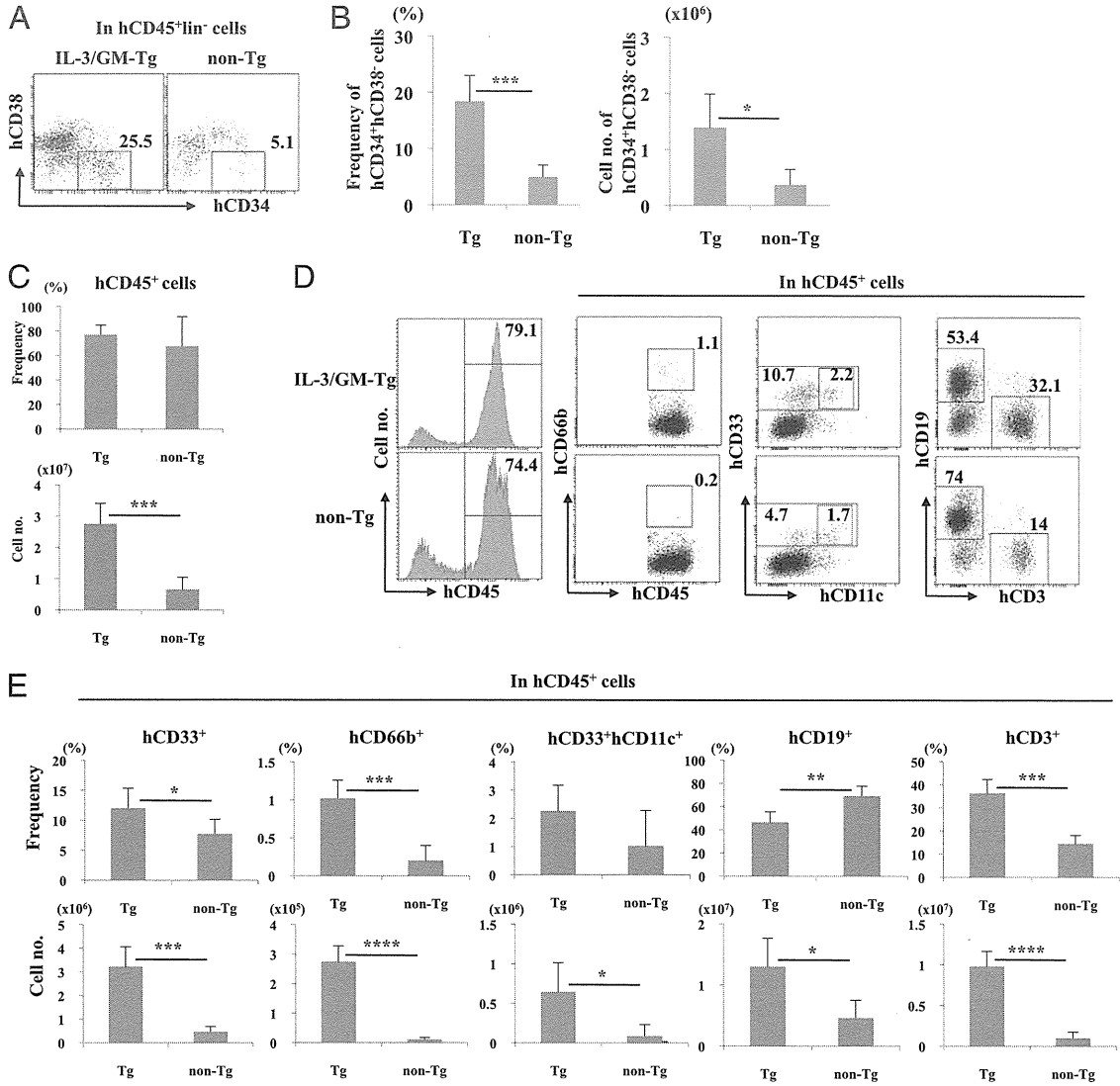

FIGURE 2. Analysis of the BM and spleen in NOG IL-3/GM–Tg mice. BM cells were isolated from the tibiae of hu-HSC NOG IL-3/GM–Tg and non-Tg mice and stained with anti-hCD34, anti-hCD38, and anti-hCD45 Abs and anti-lineage markers to identify hHSCs (hCD34$^+$hCD38$^-$ cells in the hCD45$^+$ lineage$^-$). A representative HSC staining pattern (**A**) and the mean frequency and cell numbers [(**B**), n = 5/group] are shown. (**C–E**) After the preparation of splenocytes from hu-HSC NOG–Tg and non-Tg mice at 20–22 wk postreconstitution, the total number of cells was counted, and the cells were stained with various Abs to facilitate analysis by flow cytometry. (C) Frequency (*upper panel*) and number (*lower panel*) of hCD45$^+$ human leukocytes. Data are the mean ± SD (n = 5 mice/group). (D and E) Differentiation of human myeloid and lymphoid cells in hu-HSC NOG IL-3/GM–Tg mice. After staining with Abs specific for myeloid (hCD33, hCD66b, and hCD11c) and lymphoid (hCD19 and hCD3) markers, the cells were analyzed by flow cytometry. (**D**) Representative plots. (**E**) Frequency (*upper panels*) and absolute cell number (*lower panels*) for each hCD45$^+$ cell subpopulation. Absolute cell number was calculated by multiplying the frequency by the total cell number. *$p < 0.05$, **$p < 0.005$, ***$p < 0.0005$, ****$p < 0.00005$.

fold in hu-HSC NOG IL-3/GM–Tg mice (Supplemental Fig. 1D), whereas there was no significant difference in BM cell numbers (Supplemental Fig. 1D). Overall, the numbers of myeloid cells were increased in BM and BALF samples from hu-HSC NOG IL-3/GM–Tg mice (Supplemental Fig. 1E, 1F). For lymphoid lineage cells, the T cell population was significantly larger in all tissues from hu-HSC NOG IL-3/GM–Tg mice compared with non-Tg mice in terms of both frequency and absolute cell number (Fig. 2E, Supplemental Fig. 1E, 1F). The frequency of B cells was lower in spleen and BM from hu-HSC NOG IL-3/GM–Tg mice than in non-Tg mice (Fig. 2E, Supplemental Fig. 1E). Nevertheless, the number of B cells was higher in spleen and BALF tissues from hu-HSC NOG IL-3/GM–Tg mice compared with non-Tg mice (Fig. 2E, Supplemental Fig. 1F). The increase in the total number of hCD45$^+$ cells may compensate for the reduction in the number of B cells in Tg mice. Following the marked improvement of the development of human myeloid cells, we also confirmed development of a large number of human macrophages in various tissues, including the liver, lung, and spleen, in hu-HSC NOG IL-3/GM–Tg mice (Supplemental Fig. 1G).

Taken together, these data demonstrate that human myelopoiesis, especially the development of granulocytes, was dramatically improved in NOG IL-3/GM–Tg mice.

Development of human granulocytes in hu-HSC NOG IL-3/GM–Tg mice

One of the main characteristics of HSC-transplanted NOG IL-3/GM–Tg mice was the efficient development of human granulocytes. Therefore, we examined whether these cells contain typical subpopulations (i.e., basophils, eosinophils, and neutrophils). To analyze the morphology of human granulocytes from hu-HSC NOG IL-3/GM–Tg and non-Tg mice, human leukocytes were purified from the PB by eliminating mCD45$^+$ cells. In the hCD45$^+$ cells from Tg mice, there was an SSC^{midhi}hCD66b$^+$ cell population, whereas no corresponding cell population existed in non-Tg mice (Fig. 3A). Smears of hCD45$^+$ cells from hu-HSC IL-3/GM–Tg mice, but not non-Tg mice, showed large numbers of leukocytes with intracellular granules and lobulated nuclei (Fig. 3B). At a higher magnification, we identified the cells containing red (Fig. 3C, *left panel*) or dark blue (Fig. 3C, *middle panel*) granules, which represented eosinophils and basophils, respectively. Although there also were cells whose nuclei had two lobules and small granules (Fig. 3C, *right panel*), these cells were presumably immature neutrophils. We detected no mature neutrophils with highly lobulated nuclei.

Development of mature basophils and mast cells in hu-HSC NOG IL-3/GM–Tg mice

Considering the pathogenic roles of basophils and mast cells in allergic responses, we were interested in determining whether these populations can be induced to enter a mature state in hu-HSC NOG IL-3/GM–Tg mice.

We examined whether human cells expressing FcεRI or CD203c, functional and phenotypic markers, respectively, were present. As shown in Fig. 4A, there was a clear subpopulation of hFcεRI$^+$ hCD203c$^+$ cells, which represented basophils and mast cells, in PB, BM, spleen, and BALF samples from hu-HSC NOG IL-3/GM–Tg mice but not non-Tg mice. The frequencies and numbers of hFcεRI$^+$hCD203c$^+$ cells were significantly higher in hu-HSC NOG IL-3/GM–Tg mice than in non-Tg mice (Fig. 4B). These data suggest that IL-3 and/or GM-CSF support the development of FcεR-expressing mature basophils and mast cells. We further distinguished mast cells and basophils by assessing hc-kit expression. As shown in Fig. 4C, all hFcεRI$^+$hCD203c$^+$ cells were hc-kit$^-$ (basophils) in human PBMCs. In contrast, ~20% of hFcεRI$^+$ hCD203c$^+$ cells in the PB collected from hu-HSC IL-3/GM–Tg mice were hc-kit$^+$ (mast cells; Fig. 4C). When we compared the frequencies of basophils and mast cells in various tissues, ~70 and 50% of hFcεRI$^+$hCD203c$^+$ cells in the spleen and BM, respectively, were mast cells (Fig. 4D), suggesting that these cell types were differentially distributed in various tissues. When we stimulated these hFcεRI$^+$hCD203c$^+$ mast cells or basophils in BM of IL-3/GM–Tg mice, they showed elevated expression of CD63. The levels of CD63 were as high as those of basophils in human PBMCs, representing a marker of basophil and mast cell activation (37), which suggests that these cells were functional (Fig. 4E).

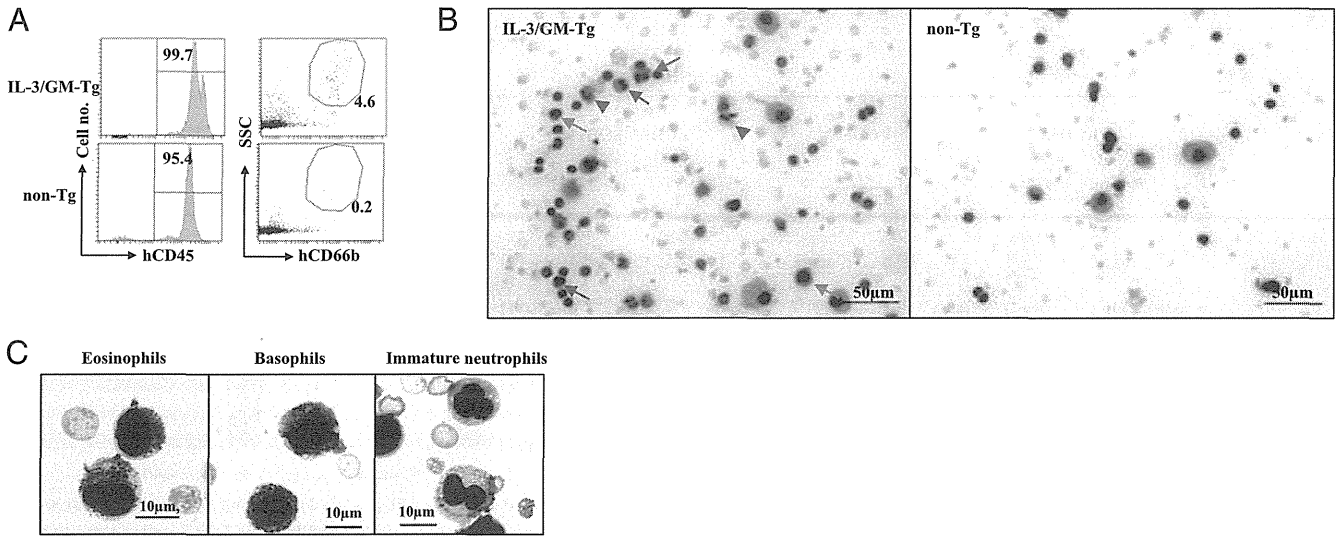

FIGURE 3. Development of human granulocytes in hu-HSC NOG IL-3/GM–Tg mice. (**A**) Human leukocytes were negatively enriched by >95% in the PB from hu-HSC NOG IL-3/GM–Tg or non-Tg mice at 11 wk after HSC transplantation. The SSC^{midhi}CD66b$^+$ fraction contained human granulocytes. (**B** and **C**) Smears of purified human leukocytes from hu-HSC NOG IL-3/GM–Tg and non-Tg mice were subjected to May–Giemsa staining. Red arrows identify eosinophils, which contained large red granules. Green arrows identify basophils, which contained small dark blue granules. Immature neutrophils were identified by small red granules (red arrowheads). (C) High magnification images of eosinophils, which contained large red granules (*left panel*); basophils, which contained small dark blue granules (*middle panel*) and immature neutrophils, which appear as small red granules (*right panel*). The data shown are representative of two independent experiments.

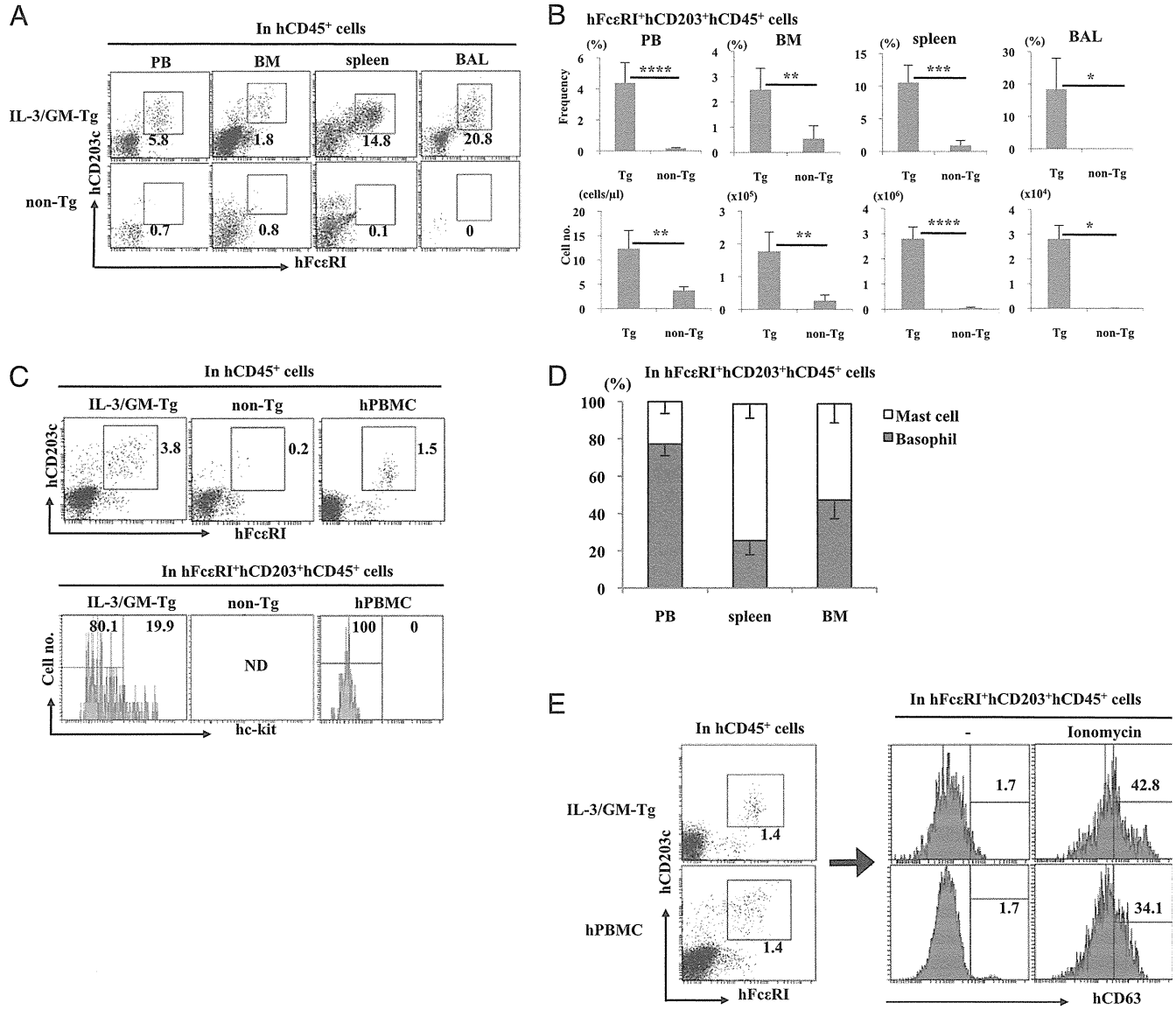

FIGURE 4. Analysis of human basophils and mast cells in hu-HSC NOG IL-3/GM–Tg mice. (**A**) Cells were isolated from PB, BM, spleen, and BALF samples from hu-HSC NOG IL-3/GM–Tg and non-Tg mice 20–22 wk after HSC transplantation and were stained with anti-hCD45, anti-hCD203c, and anti-hFcεRI Abs. The flow cytometry data are representative of five animals/group. (**B**) Cumulative data from (A). Frequency and absolute number of hFcεRI$^+$hCD203c$^+$ cells in hCD45$^+$ cells. Data are mean ± SD. (**C**) PBMCs from hu-HSC NOG IL-3/GM–Tg and non-Tg mice and hPBMCs were further stained with an anti–hc-kit Ab. The hFcεRI$^+$hCD203c$^+$ cells were analyzed for expression of hc-kit, and the data are shown as graphs (*lower panels*). The numbers in the graphs indicate the frequencies of hFcεRI$^+$hCD203c$^+$hc-kit$^-$ basophils and hFcεRI$^+$hCD203c$^+$hc-kit$^+$ mast cells. (**D**) The frequencies of human basophils and mast cells in the indicated tissues from hu-HSC NOG IL-3/GM–Tg mice were obtained as described in (C). Data are mean ± SD. (**E**) Expression of hCD63 on basophils and mast cells in hu-HSC NOG IL-3/GM–Tg mice. BM mononuclear cells were collected from two hu-HSC NOG IL-3/GM–Tg mice 18 wk after HSC transplantation and stimulated with ionomycin. Human PBMCs were used as a positive control. The cells were stained with each Ab, and the levels of hCD63 in hCD45$^+$hCD203$^+$hFcεR$^+$ cells, with or without stimulation, are presented as graphs. Representative data are shown. $*p < 0.05$, $**p < 0.005$, $***p < 0.0005$, $****p < 0.00005$.

Tissue-resident human mast cells were identified by immunohistochemistry using anti-hMCC Abs (Fig. 5A). MCC$^+$ cells were abundant in the spleen in hu-HSC NOG IL-3/GM–Tg mice, whereas only a few MCC$^+$ cells were detected in non-Tg mice. Significant numbers of MCC$^+$ cells were also identified in the lungs and stomach of hu-HSC NOG IL-3/GM–Tg mice but not non-Tg mice. Generally, human mast cells are classified on the basis of their protease contents (38). Mast cells containing tryptase and chymase (MCTC) localize primarily in the skin and any other tissues and resemble the connective tissue–type mast cells in the rodent. In contrast, mast cells containing tryptase (MCTs) but not chymase are dominant in mucosal tissues, including the lung and gastric mucosa, similar to mucosal-type mast cells in rodents. To clarify the subtypes of human mast cells, we stained sections from the spleen, lung, stomach, and skin from humanized Tg or non-Tg mice with anti-chymase and anti-tryptase mAbs. We detected abundant MCTCs with tryptase and chymase, whereas few MCTs solely expressed tryptase (Fig. 5B).

Taken together, these results suggested that a large number of IgER-expressing human basophils and mast cells developed in IL-3/GM–Tg mice. These human mast cells resemble MCTCs and are distributed in various tissues, including mucosal tissues.

PCA responses in hu-HSC NOG IL-3/GM–Tg mice

Mast cells mediate allergic responses by releasing chemical substances, such as histamine or leukotrienes. A series of intracellular

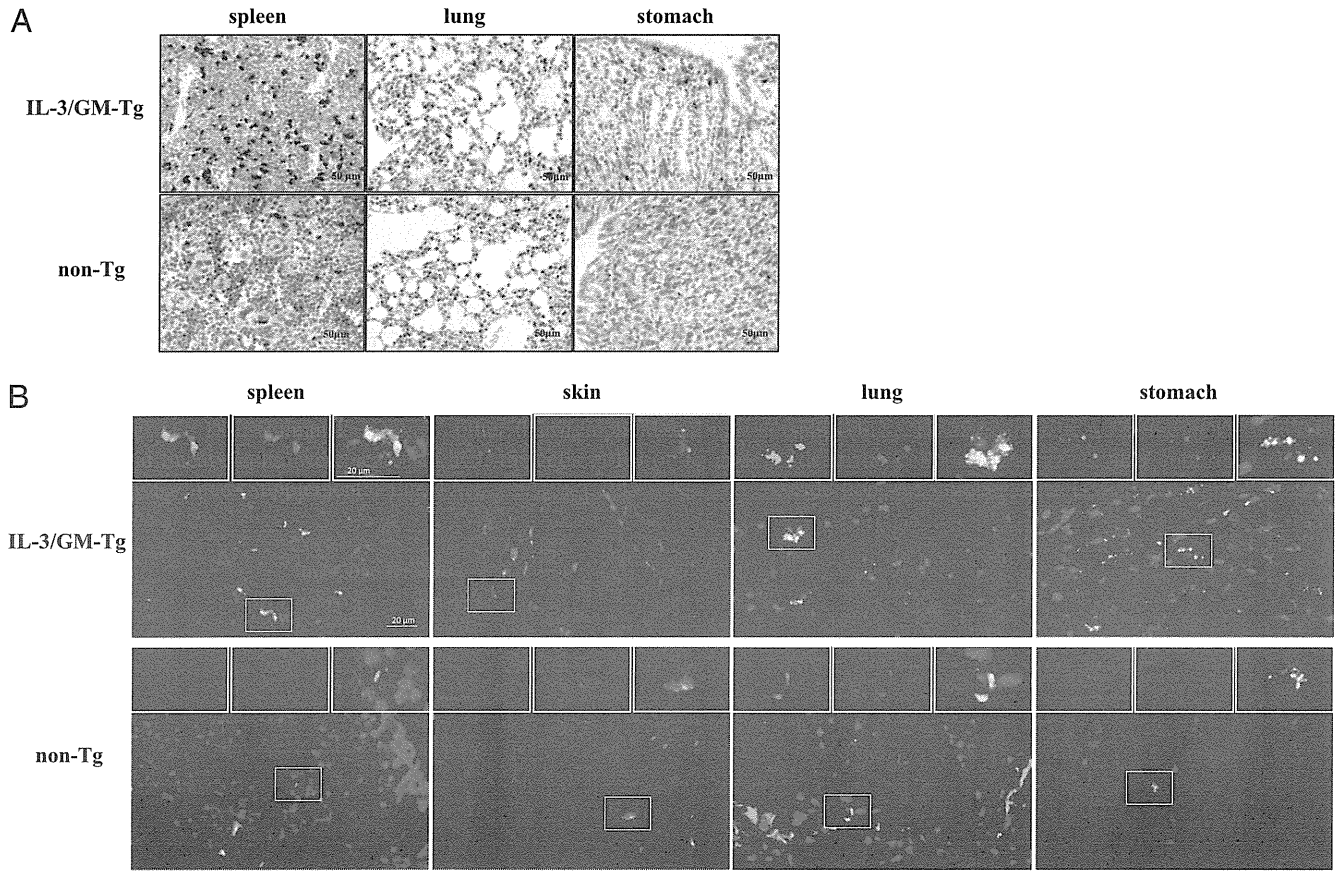

FIGURE 5. Histology of human mast cells in hu-HSC NOG IL-3/GM–Tg mice. (**A**) Detection of human mast cells by immunohistochemistry. Sections of various tissues from hu-HSC NOG IL-3/GM–Tg or non-Tg mice were stained with an anti-human MCC Ab. Each brown dot represents an individual human MCC-expressing mast cell. Representative images from five mice are shown. (**B**) Multicolor immunofluorescence analysis of human mast cells. Frozen sections of each tissue from Tg or non-Tg mice were stained with anti-human mast cell tryptase (green) and MCC (red) Abs. For double-labeled cells, the separate images were pseudo-colored, one as green and the other as red, and then merged to create the yellow color. Images shown are representative of one of three mice.

processes leading to degranulation of mast cells was triggered by cross-linking of IgE-bound FcεRI by specific Ags. The presence of a large number of human mast cells and basophils in hu-HSC NOG IL-3/GM–Tg mice prompted us to examine whether those cells could mediate Ag-specific IgE–dependent PCA reactions in vivo. Animals were sensitized with NP-specific IgE and challenged with NP-conjugated BSA 1 d later. As demonstrated in Fig. 6A, hu-HSC NOG IL-3/GM–Tg mice showed strong local inflammatory responses manifested by the extravasation of Evans blue dye, but much weaker in non-Tg mice. This was an Ag-specific reaction because the extravasation of the dye was detected only in the dorsal skin, and not on the ventral side, where control hIgE was administered. Furthermore, our examination showed that the PCA response was mediated by human cells, because nonhumanized NOG mice showed no extravasation of Evans blue dye, which eliminated the possibility that murine mast cells were activated by hIgE and hAg complexes. MCC staining confirmed the localization of a large number of human mast cells in both the dorsal and ventral skin of hu-HSC NOG IL-3/GM–Tg mice, with fewer human mast cells in non-Tg mice (Fig. 6B). Moreover, immunohistochemistry of the serial sections revealed that most of the FcεRI$^+$ cells in the dorsal skin of hu-HSC NOG IL-3/GM–Tg and non-Tg mice were positive for MCC (Fig. 6C), supporting that the PCA reaction was mediated by FcεRI-expressing human mast cells. Recently, Schafer et al. (39) demonstrated that the anaphylatoxins C3a and C5a enhance the IgE-mediated PCA reaction, including mast cell degranulation and inflammation, in mice. Indeed, we detected the expression of both hC3aR and hC5aR on mast cells in hu-HSC NOG IL-3/GM–Tg mice (Supplemental Fig. 2A). Then, to examine the role of the anaphylatoxins in our system, either C3aR or C5aR antagonist was administered to hu-HSC NOG IL-3/GM–Tg mice to inhibit binding of these anaphylatoxins on human mast cells during our NP-induced PCA responses. The PCA responses were strongly inhibited by the C3aR antagonist but not by the C5aR antagonist (Supplemental Fig. 2B, 2C). The modest effect of the C5aR antagonist may be attributed to the lack of murine C5 in NOD strains (40). These results suggest that the C3a anaphylatoxin plays an important role in the induction of PCA in hu-HSC NOG IL-3/GM–Tg mice.

We next examined whether the PCA reaction could be caused by patient-derived materials. We used the serum containing Japanese cedar pollen–specific hIgE obtained from pollinosis patients. After sensitization with the serum and subsequent injection with cedar pollen extract, strong extravasation of Evans blue dye into skin was detected in hu-HSC NOG IL-3/GM–Tg mice (Fig. 6D, 6E). Non-Tg mice showed a weak PCA reaction, probably due to the presence of only a few FcεRI$^+$ cells (Fig. 6B), which may react with hIgE (Fig. 6D, 6E).

Collectively, these results suggested that human mast cells differentiated in hu-HSC NOG IL-3/GM–Tg mice have sufficient capacity to mediate allergic inflammatory responses in vivo and that the effector phase of allergic responses manifested by histamine release can be fully recapitulated in our hu-HSC NOG IL-3/GM–Tg mice.

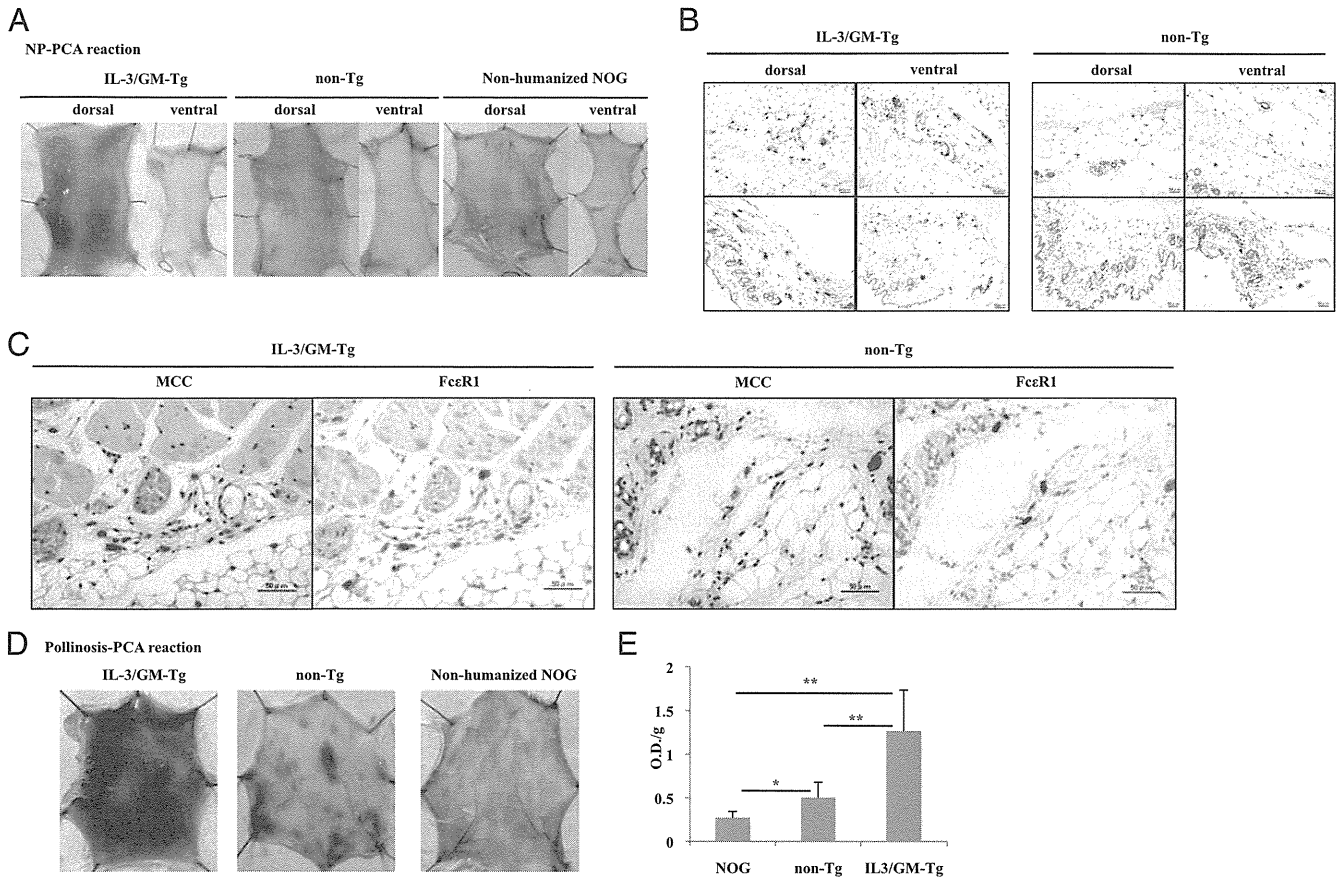

FIGURE 6. PCA reaction in hu-HSC NOG IL-3/GM–Tg mice. PCA was induced as described in *Materials and Methods*. (**A**) Extravasation of Evans blue dye in hu-HSC NOG IL-3/GM–Tg mice. Skin from dorsal (*left panels*) or ventral (*right panels*) sides was isolated from the indicated mice 30 min after systemic administration of NP and Evans blue dye. Representative images from two independent experiments using three mice are shown. (**B**) Localization of human mast cells in skin. After PCA sensitization, sections of dorsal and ventral skin from hu-HSC NOG IL-3/GM–Tg and non-Tg mice were stained with anti-human MCC Abs. Images of two fields from the indicated skin are shown. Each brown dot represents an individual human MCC-expressing mast cell. (**C**) Immunohistochemistry of the serial sections from skin. Skin samples from (B) were serially sectioned and stained with anti-human MCC and FcεRI Abs. (**D**) Extravasation of Evans blue dye in the skin of hu-HSC NOG IL-3/GM–Tg mice sensitized with the serum from Japanese cedar pollinosis patients. Dorsal skins were isolated from the hu-HSC NOG IL-3/GM–Tg (n = 6), non-Tg (n = 6), and nonhumanized NOG (n = 4) mice 30 min after systemic administration of a Japanese cedar pollen extract and Evans blue dye. Representative images of the dorsal skins are shown. (**E**) Quantification of Evans blue dye. The Evans blue dye in the skin was extracted with formamide, and the absorbance at 620 nm was measured using a spectrometer. $*p < 0.05$, $**p < 0.005$.

Discussion

In the current study, we demonstrated that a novel IL-3/GM–Tg NOG mouse substrain has a strong ability to promote the development of a variety of human myeloid cells from HSCs. Strikingly, developed human mast cells mediated allergic responses, as shown in PCA tests. To our knowledge, this is the first model to demonstrate that human cells generated in mice can mediate human allergic reactions in a reliable and repeatable manner.

Two immunodeficient mouse strains carrying the human *IL-3* and *GM-CSF* genes have been generated: IL-3/GM-CSF/SCF–Tg (SGM3-Tg) mice (30) and IL-3/GM-CSF-KI mice (41). It is noteworthy that there were considerable differences in phenotypes between our study and these previous studies. For example, in contrast to the high engraftment of hHSCs in our IL-3/GM–Tg mice, engraftment was reduced in SGM3-Tg mice compared with control mice, and there was no significant improvement in HSC engraftment in IL-3/GM–CSF–KI mice. In addition, there were no major differences in the frequency or number of macrophages, granulocytes, or T cells between IL-3/GM–CSF–KI mice and control mice. Those phenotypes were completely different from our IL-3/GM–Tg mice, which have the highest potential of these three strains from the point of view of HSC maintenance and myelopoiesis. These inconsistencies may be attributed, in part, to differences in the levels and distributions of cytokines. The amount of IL-3 was 4–6-fold higher in SGM3-Tg mice than in our IL-3/GM–Tg mice. Because high levels of IL-3 interfere with HSC proliferation, despite its pivotal role in the expansion of HSCs in in vitro culture systems (42), this increase in IL-3 in SGM3-Tg mice may explain the reduction in HSCs in SGM3-Tg mice. In IL-3/GM–CSF–KI mice, the expression patterns of hIL-3 and hGM-CSF were similar to those of endogenous mIL-3 and mGM-CSF. Accordingly, because of the high expression of GM-CSF, major effects were most evident in the lungs, where many human alveolar macrophages resided after HSC transplantation. Hence, the tissue-specific expression of IL-3 or GM-CSF in KI mice was sufficient for tissue-specific development and migration of human cells but not for systemically reconstituting entire human myeloid cells.

Intriguingly, the improved development of myeloid cells in our IL-3/GM–Tg mice was rather similar to that in the TPO-KI mice established by Rongvaux et al. (31), which also showed high engraftment of HSCs, enhanced myeloid cell development, and granulocyte differentiation. Although detailed analyses of granulocyte subpopulations have not been reported in TPO-KI mice,

Giemsa staining indicated the differentiation of neutrophil-like cells with highly lobulated nuclei, which were rarely detected in our IL-3/GM–Tg strain. Differences in cytokines (i.e., TPO versus IL-3/GM–CSF) influenced the lineage decisions of human myeloid cells, explaining the different results observed in these two strains.

The most striking characteristic of our NOG IL-3/GM–Tg strain was that a large number of fully functional human basophils and mast cells were able to develop from HSCs. The numbers of these cell populations in conventional humanized mice are too small in which to analyze the functional maturity and characteristics of these populations, especially in in vivo situations, although two reports demonstrated the presence of these cells in conventional NOG mice (43, 44). The initial study of human mast cells in humanized mice was reported by Kambe et al. (43). They showed that a few MCTs were present in the lung and stomach of conventional humanized NOG mice and that both types of human mast cells were differentiated in these animals. This result is inconsistent with our findings, and there might be several reasons for the discrepancy. Kambe et al. (43) identified these mast cell phenotypes by an immunoenzyme technique using anti-chymase (clone: B7) and anti-tryptase (clone: G3) mAbs, whereas we used directly labeled mAbs for our double-staining results. These different techniques and mAb clones could explain this inconsistency. Also, MCTs require IL-4 to suppress chymase expression (45). The production of IL-4 from human T cells in humanized mice was markedly lower than that in human PB, and there were large variances in the amounts of IL-4 in humanized mice (46). Varying levels of IL-4 may be responsible for the poor development of MCTs in our mouse colony. Therefore, administration of hIL-4 to humanized mice may support human mast cell development.

Recently, Takagi et al. (32) demonstrated that the development of human mast cells was significantly improved in their new hSCF-Tg NSG strain compared with normal NSG mice. However, the expression of hFcεRI on mast cells was not evaluated, and the ability of their strain to mediate human allergic responses in vivo was not addressed. Although IL-3/GM–Tg mice have no source of hSCF, the human mast cells developed in our IL-3/GM–Tg mice may be stimulated by mSCF, which is known to cross-react with human c-kit on mast cells (24). It will be interesting to compare the development of human mast cells between IL-3/GM–Tg and SCF-Tg mice, because this comparison may be useful in future investigations of human mast cells.

Previously, hIgE-mediated allergic responses were studied using hPBMC-engrafted mice (47–49). Weigmann et al. (49) demonstrated that colon inflammation was induced by rectal or oral challenge of allergens in NSG mice transplanted with allergic patient–derived hPBMCs. In these models, it is thought that patient-derived B cells produced an allergen-specific IgE Ab in mice, which, in turn, triggered allergic inflammation upon administration of the specific allergen. Although some aspects of allergic symptoms were mimicked in these models, suggesting that they may serve as an attractive model for human allergies, there are several caveats to the current study. For example, the release of histamine and any granules would become insufficient because of the small number of human basophils or mast cells in hPBMC grafts. In addition, xenogenic GVHD occurred easily in NOD-*scid*-IL2rγ^{null} mice when they were transplanted with hPBMCs (15). Xenogenic GVHD symptoms may sometimes be confused with allergic inflammation, and careful examinations are necessary. From these points, we conclude that our IL-3/GM–Tg mouse system is superior to PBMC-induced models because of the stable presence of many human mast cells and basophils in mouse environments; moreover, these cells did not develop GVHD, enabling long-term experimentation.

In summary, we generated a novel mouse strain, IL-3/GM–CSF–Tg NOG, which is one of the most suitable strains for inducing human hematopoiesis, including the production of granulocytes and mast cells, from HSCs. In addition, it is of note that the effector phase of the human allergic response was induced by in vivo–developed human mast cells. This new mouse strain will be an indispensable platform for analyzing human allergies in vivo. Furthermore, by combining this strain with other Tg strains expressing HLA, IL-4, or IL-21, the complete recapitulation of human allergies will be possible in humanized mice. These models will enable the analysis of cellular and molecular mechanisms responsible for allergies and may become useful tools for developing antiallergy drugs in the near future.

Acknowledgments

We thank Kazuho Wakui (WDB Co., Ltd., Tokyo, Japan) and Masashi Sasaki (JAC, Inc., Tokyo, Japan) for technical assistance, and Yu-you Ka (CIEA) and Yasuhiko Ando, Takuma Mizusawa, and Kayo Tomiyama (JAC, Inc.) for maintaining the animals.

Disclosures

The authors have no financial conflicts of interest.

References

1. Kotani, M., M. Matsumoto, A. Fujita, S. Higa, W. Wang, M. Suemura, T. Kishimoto, and T. Tanaka. 2000. Persimmon leaf extract and astragalin inhibit development of dermatitis and IgE elevation in NC/Nga mice. *J. Allergy Clin. Immunol.* 106: 159–166.
2. Iwata, A., K. Nishio, R. K. Winn, E. Y. Chi, W. R. Henderson, Jr., and J. M. Harlan. 2003. A broad-spectrum caspase inhibitor attenuates allergic airway inflammation in murine asthma model. *J. Immunol.* 170: 3386–3391.
3. Tsunematsu, M., T. Yamaji, D. Kozutsumi, R. Murakami, S. Kimura, and K. Kino. 2007. Establishment of an allergic rhinitis model in mice for the evaluation of nasal symptoms. *Life Sci.* 80: 1388–1394.
4. Roy, K., H. Q. Mao, S. K. Huang, and K. W. Leong. 1999. Oral gene delivery with chitosan–DNA nanoparticles generates immunologic protection in a murine model of peanut allergy. *Nat. Med.* 5: 387–391.
5. Li, X. M., G. Kleiner, C. K. Huang, S. Y. Lee, B. Schofield, N. A. Soter, and H. A. Sampson. 2001. Murine model of atopic dermatitis associated with food hypersensitivity. *J. Allergy Clin. Immunol.* 107: 693–702.
6. Bankert, R. B., S. V. Balu-Iyer, K. Odunsi, L. D. Shultz, R. J. Kelleher, Jr., J. L. Barnas, M. Simpson-Abelson, R. Parsons, and S. J. Yokota. 2011. Humanized mouse model of ovarian cancer recapitulates patient solid tumor progression, ascites formation, and metastasis. *PLoS ONE* 6: e24420.
7. Machida, K., H. Suemizu, K. Kawai, T. Ishikawa, R. Sawada, Y. Ohnishi, and T. Tsuchiya. 2009. Higher susceptibility of NOG mice to xenotransplanted tumors. *J. Toxicol. Sci.* 34: 123–127.
8. Suemizu, H., M. Monnai, Y. Ohnishi, M. Ito, N. Tamaoki, and M. Nakamura. 2007. Identification of a key molecular regulator of liver metastasis in human pancreatic carcinoma using a novel quantitative model of metastasis in NOD/SCID/gammacnull (NOG) mice. *Int. J. Oncol.* 31: 741–751.
9. Miyakawa, Y., Y. Ohnishi, M. Tomisawa, M. Monnai, K. Kohmura, Y. Ueyama, M. Ito, Y. Ikeda, M. Kizaki, and M. Nakamura. 2004. Establishment of a new model of human multiple myeloma using NOD/SCID/gammac(null) (NOG) mice. *Biochem. Biophys. Res. Commun.* 313: 258–262.
10. Libby, S. J., M. A. Brehm, D. L. Greiner, L. D. Shultz, M. McClelland, K. D. Smith, B. T. Cookson, J. E. Karlinsey, T. L. Kinkel, S. Porwollik, et al. 2010. Humanized nonobese diabetic-scid IL2rgammanull mice are susceptible to lethal *Salmonella typhi* infection. *Proc. Natl. Acad. Sci. USA* 107: 15589–15594.
11. Sato, K., N. Misawa, C. Nie, Y. Satou, D. Iwakiri, M. Matsuoka, R. Takahashi, K. Kuzushima, M. Ito, K. Takada, and Y. Koyanagi. 2011. A novel animal model of Epstein-Barr virus-associated hemophagocytic lymphohistiocytosis in humanized mice. *Blood* 117: 5663–5673.
12. Yajima, M., K. Imadome, A. Nakagawa, S. Watanabe, K. Terashima, H. Nakamura, M. Ito, N. Shimizu, M. Honda, N. Yamamoto, and S. Fujiwara. 2008. A new humanized mouse model of Epstein-Barr virus infection that reproduces persistent infection, lymphoproliferative disorder, and cell-mediated and humoral immune responses. *J. Infect. Dis.* 198: 673–682.
13. Sato, K., T. Izumi, N. Misawa, T. Kobayashi, Y. Yamashita, M. Ohmichi, M. Ito, A. Takaori-Kondo, and Y. Koyanagi. 2010. Remarkable lethal G-to-A mutations in vif-proficient HIV-1 provirus by individual APOBEC3 proteins in humanized mice. *J. Virol.* 84: 9546–9556.
14. Watanabe, S., K. Terashima, S. Ohta, S. Horibata, M. Yajima, Y. Shiozawa, M. Z. Dewan, Z. Yu, M. Ito, T. Morio, et al. 2007. Hematopoietic stem cell-engrafted NOD/SCID/IL2Rgamma null mice develop human lymphoid systems and induce long-lasting HIV-1 infection with specific humoral immune responses. *Blood* 109: 212–218.

15. Ito, R., I. Katano, K. Kawai, H. Hirata, T. Ogura, T. Kamisako, T. Eto, and M. Ito. 2009. Highly sensitive model for xenogenic GVHD using severe immunodeficient NOG mice. *Transplantation* 87: 1654–1658.
16. van Rijn, R. S., E. R. Simonetti, A. Hagenbeek, M. C. Hogenes, R. A. de Weger, M. R. Canninga-van Dijk, K. Weijer, H. Spits, G. Storm, L. van Bloois, et al. 2003. A new xenograft model for graft-versus-host disease by intravenous transfer of human peripheral blood mononuclear cells in RAG2$^{-/-}$ gammac$^{-/-}$ double-mutant mice. *Blood* 102: 2522–2531.
17. Ito, M., H. Hiramatsu, K. Kobayashi, K. Suzue, M. Kawahata, K. Hioki, Y. Ueyama, Y. Koyanagi, K. Sugamura, K. Tsuji, et al. 2002. NOD/SCID/gamma (c)(null) mouse: an excellent recipient mouse model for engraftment of human cells. *Blood* 100: 3175–3182.
18. Hiramatsu, H., R. Nishikomori, T. Heike, M. Ito, K. Kobayashi, K. Katamura, and T. Nakahata. 2003. Complete reconstitution of human lymphocytes from cord blood CD34+ cells using the NOD/SCID/gammacnull mice model. *Blood* 102: 873–880.
19. Yahata, T., K. Ando, Y. Nakamura, Y. Ueyama, K. Shimamura, N. Tamaoki, S. Kato, and T. Hotta. 2002. Functional human T lymphocyte development from cord blood CD34+ cells in nonobese diabetic/Shi-scid, IL-2 receptor gamma null mice. *J. Immunol.* 169: 204–209.
20. Shultz, L. D., B. L. Lyons, L. M. Burzenski, B. Gott, X. Chen, S. Chaleff, M. Kotb, S. D. Gillies, M. King, J. Mangada, et al. 2005. Human lymphoid and myeloid cell development in NOD/LtSz-scid IL2R gamma null mice engrafted with mobilized human hemopoietic stem cells. *J. Immunol.* 174: 6477–6489.
21. Traggiai, E., L. Chicha, L. Mazzucchelli, L. Bronz, J. C. Piffaretti, A. Lanzavecchia, and M. G. Manz. 2004. Development of a human adaptive immune system in cord blood cell-transplanted mice. *Science* 304: 104–107.
22. Goldman, J. P., M. P. Blundell, L. Lopes, C. Kinnon, J. P. Di Santo, and A. J. Thrasher. 1998. Enhanced human cell engraftment in mice deficient in RAG2 and the common cytokine receptor gamma chain. *Br. J. Haematol.* 103: 335–342.
23. Ito, M., K. Kobayashi, and T. Nakahata. 2008. NOD/Shi-scid IL2rgamma(null) (NOG) mice more appropriate for humanized mouse models. *Curr. Top. Microbiol. Immunol.* 324: 53–76.
24. Manz, M. G. 2007. Human-hemato-lymphoid-system mice: opportunities and challenges. *Immunity* 26: 537–541.
25. Egeland, T., R. Steen, H. Quarsten, G. Gaudernack, Y. C. Yang, and E. Thorsby. 1991. Myeloid differentiation of purified CD34+ cells after stimulation with recombinant human granulocyte-monocyte colony-stimulating factor (CSF), granulocyte-CSF, monocyte-CSF, and interleukin-3. *Blood* 78: 3192–3199.
26. Brugger, W., W. Möcklin, S. Heimfeld, R. J. Berenson, R. Mertelsmann, and L. Kanz. 1993. Ex vivo expansion of enriched peripheral blood CD34+ progenitor cells by stem cell factor, interleukin-1 beta (IL-1 beta), IL-6, IL-3, interferon-gamma, and erythropoietin. *Blood* 81: 2579–2584.
27. Petzer, A. L., P. W. Zandstra, J. M. Piret, and C. J. Eaves. 1996. Differential cytokine effects on primitive (CD34+CD38−) human hematopoietic cells: novel responses to Flt3-ligand and thrombopoietin. *J. Exp. Med.* 183: 2551–2558.
28. Ohmizono, Y., H. Sakabe, T. Kimura, S. Tanimukai, T. Matsumura, H. Miyazaki, S. D. Lyman, and Y. Sonoda. 1997. Thrombopoietin augments ex vivo expansion of human cord blood-derived hematopoietic progenitors in combination with stem cell factor and flt3 ligand. *Leukemia* 11: 524–530.
29. Piacibello, W., L. Fubini, F. Sanavio, M. F. Brizzi, A. Severino, L. Garetto, A. Stacchini, L. Pegoraro, and M. Aglietta. 1995. Effects of human FLT3 ligand on myeloid leukemia cell growth: heterogeneity in response and synergy with other hematopoietic growth factors. *Blood* 86: 4105–4114.
30. Billerbeck, E., W. T. Barry, K. Mu, M. Dorner, C. M. Rice, and A. Ploss. 2011. Development of human CD4+FoxP3+ regulatory T cells in human stem cell factor-, granulocyte-macrophage colony-stimulating factor-, and interleukin-3-expressing NOD-SCID IL2Rγ(null) humanized mice. *Blood* 117: 3076–3086.
31. Rongvaux, A., T. Willinger, H. Takizawa, C. Rathinam, W. Auerbach, A. J. Murphy, D. M. Valenzuela, G. D. Yancopoulos, E. E. Eynon, S. Stevens, et al. 2011. Human thrombopoietin knockin mice efficiently support human hematopoiesis in vivo. *Proc. Natl. Acad. Sci. USA* 108: 2378–2383.
32. Takagi, S., Y. Saito, A. Hijikata, S. Tanaka, T. Watanabe, T. Hasegawa, S. Mochizuki, J. Kunisawa, H. Kiyono, H. Koseki, et al. 2012. Membrane-bound human SCF/KL promotes in vivo human hematopoietic engraftment and myeloid differentiation. *Blood* 119: 2768–2777.
33. Fukuchi, Y., Y. Miyakawa, M. Kizaki, A. Umezawa, K. Shimamura, K. Kobayashi, T. Kuramochi, J. Hata, Y. Ikeda, N. Tamaoki, et al. 1999. Human acute myeloblastic leukemia-ascites model using the human GM-CSF- and IL-3-releasing transgenic SCID mice. *Ann. Hematol.* 78: 223–231.
34. Pawankar, R., M. Okuda, H. Yssel, K. Okumura, and C. Ra. 1997. Nasal mast cells in perennial allergic rhinitics exhibit increased expression of the Fc epsilonRI, CD40L, IL-4, and IL-13, and can induce IgE synthesis in B cells. *J. Clin. Invest.* 99: 1492–1499.
35. Yamaguchi, M., K. Sayama, K. Yano, C. S. Lantz, N. Noben-Trauth, C. Ra, J. J. Costa, and S. J. Galli. 1999. IgE enhances Fc epsilon receptor I expression and IgE-dependent release of histamine and lipid mediators from human umbilical cord blood-derived mast cells: synergistic effect of IL-4 and IgE on human mast cell Fc epsilon receptor I expression and mediator release. *J. Immunol.* 162: 5455–5465.
36. Suemizu, H., C. Yagihashi, T. Mizushima, T. Ogura, T. Etoh, K. Kawai, and M. Ito. 2008. Establishing EGFP congenic mice in a NOD/Shi-scid IL2Rg(null) (NOG) genetic background using a marker-assisted selection protocol (MASP). *Exp. Anim.* 57: 471–477.
37. Knol, E. F., F. P. Mul, H. Jansen, J. Calafat, and D. Roos. 1991. Monitoring human basophil activation via CD63 monoclonal antibody 435. *J. Allergy Clin. Immunol.* 88: 328–338.
38. Irani, A. A., N. M. Schechter, S. S. Craig, G. DeBlois, and L. B. Schwartz. 1986. Two types of human mast cells that have distinct neutral protease compositions. *Proc. Natl. Acad. Sci. USA* 83: 4464–4468.
39. Schafer, B., A. M. Piliponsky, T. Oka, C. H. Song, N. P. Gerard, C. Gerard, M. Tsai, J. Kalesnikoff, and S. J. Galli. 2013. Mast cell anaphylatoxin receptor expression can enhance IgE-dependent skin inflammation in mice. *J. Allergy Clin. Immunol.* 131: 541–548.e1–9.
40. Lynch, D. M., and P. H. Kay. 1995. Studies on the polymorphism of the fifth component of complement in laboratory mice. *Exp. Clin. Immunogenet.* 12: 253–260.
41. Willinger, T., A. Rongvaux, H. Takizawa, G. D. Yancopoulos, D. M. Valenzuela, A. J. Murphy, W. Auerbach, E. E. Eynon, S. Stevens, M. G. Manz, and R. A. Flavell. 2011. Human IL-3/GM-CSF knock-in mice support human alveolar macrophage development and human immune responses in the lung. *Proc. Natl. Acad. Sci. USA* 108: 2390–2395.
42. Zandstra, P. W., E. Conneally, A. L. Petzer, J. M. Piret, and C. J. Eaves. 1997. Cytokine manipulation of primitive human hematopoietic cell self-renewal. *Proc. Natl. Acad. Sci. USA* 94: 4698–4703.
43. Kambe, N., H. Hiramatsu, M. Shimonaka, H. Fujino, R. Nishikomori, T. Heike, M. Ito, K. Kobayashi, Y. Ueyama, N. Matsuyoshi, et al. 2004. Development of both human connective tissue-type and mucosal-type mast cells in mice from hematopoietic stem cells with identical distribution pattern to human body. *Blood* 103: 860–867.
44. Tanaka, S., Y. Saito, J. Kunisawa, Y. Kurashima, T. Wake, N. Suzuki, L. D. Shultz, H. Kiyono, and F. Ishikawa. 2012. Development of mature and functional human myeloid subsets in hematopoietic stem cell-engrafted NOD/SCID/IL2rγKO mice. *J. Immunol.* 188: 6145–6155.
45. Lorentz, A., and S. C. Bischoff. 2001. Regulation of human intestinal mast cells by stem cell factor and IL-4. *Immunol. Rev.* 179: 57–60.
46. Saito, Y., Y. Kametani, K. Hozumi, N. Mochida, K. Ando, M. Ito, T. Nomura, Y. Tokuda, H. Makuuchi, T. Tajima, and S. Habu. 2002. The in vivo development of human T cells from CD34(+) cells in the murine thymic environment. *Int. Immunol.* 14: 1113–1124.
47. Duez, C., A. Tsicopoulos, A. Janin, I. Tillie-Leblond, G. Thyphronitis, P. Marquillies, Q. Hamid, B. Wallaert, A. B. Tonnel, and J. Pestel. 1996. An in vivo model of allergic inflammation: pulmonary human cell infiltrate in allergen-challenged allergic Hu-SCID mice. *Eur. J. Immunol.* 26: 1088–1093.
48. Herz, U., V. A. Botchkarev, R. Paus, and H. Renz. 2004. Increased airway responsiveness, allergy-type-I skin responses and systemic anaphylaxis in a humanized-severe combined immuno-deficiency mouse model. *Clin. Exp. Allergy* 34: 478–487.
49. Weigmann, B., N. Schughart, C. Wiebe, S. Sudowe, H. A. Lehr, H. Jonuleit, L. Vogel, C. Becker, M. F. Neurath, S. Grabbe, et al. 2012. Allergen-induced IgE-dependent gut inflammation in a human PBMC-engrafted murine model of allergy. *J. Allergy Clin. Immunol.* 129: 1126–1135.

Vaccine 32 (2014) 864–871

Contents lists available at ScienceDirect

Vaccine

journal homepage: www.elsevier.com/locate/vaccine

Tricomponent fusion complex comprising a viral antigen, a pentameric α-helical coiled-coil, and an immunoglobulin-binding domain as an effective antiviral vaccine

Takeshi Arakawa[a,b,*], Tetsuya Harakuni[a], Takeshi Miyata[a], Senji Tafuku[c], Masayuki Tadano[d]

[a] Molecular Microbiology Group, Department of Tropical Infectious Diseases, COMB, Tropical Biosphere Research Center, University of the Ryukyus, 1 Senbaru, Nishihara, Okinawa 903-0213, Japan
[b] Division of Host Defense and Vaccinology, Department of Microbiology, Graduate School of Medicine, University of the Ryukyus, 207 Uehara, Nishihara, Okinawa 903-0215, Japan
[c] Jectas Innovators Co. Ltd., 1 Senbaru, Nishihara, Okinawa 903-0213, Japan
[d] Department of Molecular Virology, Graduate School of Medicine, University of the Ryukyus, 207 Uehara, Nishihara, Okinawa 903-0215, Japan

ARTICLE INFO

Article history:
Received 26 August 2013
Received in revised form 5 December 2013
Accepted 10 December 2013
Available online 24 December 2013

Keywords:
Japanese encephalitis virus E protein
α-Helical coiled-coil
Cartilage oligomeric matrix protein
Delivery system
Vaccine

ABSTRACT

The pentameric coiled-coil domain of cartilage oligomeric matrix protein (COMP) genetically fused to the Z domain of *Staphylococcus aureus* protein A, an immunoglobulin-binding domain (IBD), was evaluated as a viral antigen carrier complex. In a proof-of-concept study, recombinant Japanese encephalitis virus (JEV) E protein domain III (D3) was loaded onto the COMP–Z fusion protein by chemical conjugation, and the tricomponent complex generated, COMP–Z/D3, was evaluated for its vaccine efficacy in a mouse JEV infection model. Immunization with the complex conferred substantially greater protection against lethal JEV infection than the unloaded antigen. Next, a tricomponent complex was engineered in which the three molecular entities (the D3 antigen, COMP coiled-coil domain, and Z domain) were genetically connected in tandem to create the D3–COMP–Z tricomponent complex, or its reversal oriented construct, Z–COMP–D3. The fusion complexes were produced as inclusion bodies in *Escherichia coli*, but could be refolded to biologically active pentamers that retained the E protein antigenicity and the IBD function. Immunization with the refolded complexes conferred a high level of protection against lethal JEV infection, similar in efficacy to that of the tricomponent complex generated by chemical conjugation. These results demonstrate that the tricomponent complex, whether generated by chemical or genetic fusion, is a promising molecular design for the creation of effective subunit vaccines against viral infections.

1. Introduction

Innocuous protein antigens can become effective vaccines against infectious diseases if their immunogenicity is strongly augmented. For this reason, their coadministration with adjuvants, which induce innate immunity, is the most practical approach to eliciting the adaptive immunity represented by antibody and/or cell-mediated immune responses. Although oil-based adjuvants are promising, they often induce unacceptable reactogenicity, which may lead to the discontinuation of vaccine development. Therefore, the use of moderately strong adjuvants with robust safety, such as those based on aluminum salts (alum), combined with recombinant protein engineering techniques may be a desirable alternative strategy for vaccine design. Specific delivery of antigens to professional antigen-presenting cells (APCs) is one such promising technique [1–3], and when combined with alum adjuvants, may induce a sufficiently strong immune response to effectively control infections.

We recently reported novel antigen delivery molecules that were shown to target B lymphocytes and to robustly augment the immunogenicity of loaded recombinant protein antigens [4]. The delivery system exploits three physically linked molecular entities: (1) a recombinant protein antigen; (2) an APC-targeting ligand; and (3) a multimer-forming antigen scaffold. In our previous study, we created a prototype molecule in which the α-helical coiled-coil domain of cartilage oligomeric matrix protein (COMP) [5] was genetically linked to the Z domain [6], a derivative of the D domain of *Staphylococcus aureus* protein A [4]. The fusion gene was expressed extracellularly by *Escherichia coli* as a pentamer, onto which vaccine candidate antigens of the malarial parasite were

* Corresponding author at: Molecular Microbiology Group, Tropical Biosphere Research Center, COMB, University of the Ryukyus, 1 Senbaru, Nishihara, Okinawa 903-0213, Japan. Tel.: +81 98 895 8974; fax: +81 98 895 8974.
E-mail address: tarakawa@comb.u-ryukyu.ac.jp (T. Arakawa).

0264-410X/$ – see front matter © 2014 Elsevier Ltd. All rights reserved.
http://dx.doi.org/10.1016/j.vaccine.2013.12.016

loaded by chemical conjugation. The tricomponent complexes thus generated were shown to induce robust antiparasitic immunity [4].

In this proof-of-concept study to evaluate the vaccine efficacy of the tricomponent complex against viral infections, we exploited a mouse infection model of Japanese encephalitis (JE). We have previously reported that the recombinantly produced envelope (E) protein of the JE virus (JEV) confers substantial protection against lethal JEV infection in mice [7]. In this study, we expressed the C-terminal one-third of the E protein (domain III [D3]) in *E. coli* and loaded it onto the COMP–Z fusion protein by chemical conjugation. We also created a tricomponent fusion complex in which the D3 antigen, COMP coiled-coil domain, and Z domain were genetically connected in sequence. We then evaluated the vaccine efficacy of the tricomponent complex generated either by chemical or genetic fusion, using a mouse model of lethal JEV infection.

2. Materials and methods

2.1. Production of COMP–Z/D3 tricomponent complex by chemical conjugation

The expression and purification of the JEV E protein D3 and COMP–Z fusion proteins from *E. coli* were as described previously [4,7]. Briefly, purified D3 was pyridyldithiol activated with *N*-succinimidyl 3-(2-pyridyldithio) propionate (SPDP; 0.6 mM; Thermo Scientific, Inc., Rockford, IL, USA). Concomitantly, the COMP–Z fusion protein was treated with dithiothreitol (DTT; 50 mM) to reduce the disulfide bonds located in the COMP coiled-coil domain. The modified D3 and COMP–Z were mixed in a 10:1 molar ratio at a total protein concentration of 1 mg/ml. The generated fusion complex was evaluated with a human IgG enzyme-linked immunosorbent assay (human IgG ELISA).

2.2. Production of D3–COMP–Z and Z–COMP–D3 tricomponent complexes by genetic fusion

First, the COMP-spacer coding region located between the *Nco*I and *Xho*I sites of the pET-22b vector (Merck KGaA, Darmstadt, Germany), described previously [4], was excised with the *Nco*I and *Xho*I restriction endonucleases and subcloned between the corresponding sites of the pET-21d vector (Merck KGaA). This subcloning removed the pelB signal from the COMP-spacer coding region. Next, to construct the pET-21d–Spacer1–COMP–Spacer2 expression plasmid (Figs. 2a and 3a), two overlapping oligonucleotides encoding the Spacer1 region (#1 sense and #2 antisense oligonucleotides) were annealed and subcloned at the unique *Nco*I site on the formerly constructed pET-21d–COMP–spacer expression plasmid. The two overlapping oligonucleotides were designed to generate an *Nco*I staggered end at the N-terminus but not at the C-terminus of the Spacer1 coding region, to reconstitute a unique *Nco*I site in the vector to allow further subcloning of the JEV D3 or Z domain, as described below.

Second, the JEV D3 coding region was PCR amplified from a plasmid containing the JEV (strain Beijing-1; GenBank accession no. L48961) E protein coding region [7] using a set of primers (#3 sense and #4 antisense oligonucleotide set containing an *Nco*I site or #5 sense and #6 antisense oligonucleotide set containing an *Xho*I site). The PCR-amplified fragment was subcloned into the pCR2.1 vector (Invitrogen, Carlsbad, CA, USA), and then digested with *Nco*I or *Xho*I. The excised fragment was subcloned at the *Nco*I or *Xho*I site on the formerly constructed pET-21d–Spacer1–COMP–Spacer2 expression plasmid (Figs. 2a and 3a) to create the D3–COMP–Spacer2 or Spacer1–COMP–D3 coding region, respectively.

Third, a synthetic gene encoding the Z domain (Val1 to Lys58; Protein Data Bank accession no. 2SPZ) was PCR amplified from a plasmid containing the corresponding gene [4] using a set of primers (#7 sense and #8 antisense oligonucleotide set containing an *Xho*I site or #9 sense and #10 antisense oligonucleotide set containing an *Nco*I site). The amplified fragment was subcloned into pCR2.1, and then digested with *Xho*I or *Nco*I. The excised fragment was subcloned at the *Xho*I site on the formerly constructed pET-21d–D3–COMP–Spacer2 expression plasmid or the *Nco*I site on the pET-21d–Spacer1–COMP–D3 expression plasmid to create the D3–COMP–Z or Z–COMP–D3 coding region, respectively. Table 1 lists the oligonucleotides used in this study. The correctness of the nucleotide sequences of the constructed fusion genes was confirmed by DNA sequencing.

E. coli BL21(DE3) harboring the pET-21d–D3–COMP–Z or pET-21d–Z–COMP–D3 expression plasmid was cultured in LB broth containing ampicillin (100 μg/mL), and the protein expression was induced with 1 mM isopropylthio-β-galactoside (IPTG) for 16 h. After induction, the cells were collected by centrifugation (9600 × *g*, 30 min), and resuspended in phosphate-buffered saline (PBS). The cells were disrupted by sonication (20 min × 3; Output 4, Duty 70, Tomy UD-201, Tomy Seiko Co. Ltd., Tokyo, Japan), and centrifuged (10,000 × *g*, 30 min) to collect the inclusion bodies. The inclusion bodies were dissolved in 8 M urea and centrifuged (10,000 × *g*, 30 min) to remove the insoluble debris. The protein solution dissolved in 8 M urea was dialyzed stepwise against decreasing concentrations of urea (8–1 M) and finally against PBS. The dialyzed samples were evaluated with a human IgG ELISA and size-exclusion chromatography (0.8 ml/min flow rate, HiLoad 16/60 Superdex 75 pg column; GE Healthcare, Little Chalfont, UK), as previously described [4]. Final recombinant protein yield was determined by bicinchoninic acid (BCA) assay. Protein samples which were PBS-exchanged, and then size-fractionated by size-exclusion chromatography (i.e., pentameric as well as high-molecular mass protein fractions), or unfractionated protein samples were used for human IgG ELISA experiments or mouse immunization studies.

2.3. Human IgG ELISA

Human IgG ELISA was conducted as previously described with a slight modification [4]. Briefly, 5 μg/ml human IgG (Sigma–Aldrich, St. Louis, MO, USA), diluted with bicarbonate buffer (15 mM Na_2CO_3, 35 mM $NaHCO_3$, pH 9.6; 50 μl/well), was applied to a 96-well microtiter plate (Sumilon; Sumitomo Bakelite Co., Ltd., Tokyo, Japan) and incubated at 4 °C overnight. The plate was blocked with 10% skim milk in PBS for 1 h at 37 °C. Chemically or genetically produced tricomponent protein samples (2 μg total protein/well) were added to the wells and incubated at 37 °C for 1 h, and then incubated with 50 μg/ml human IgG at 37 °C for 1 h to mask any unbound free Z domain. Mouse anti-His tag antibody (1:4000; GE Healthcare) or mouse anti-D3 antiserum (1:4000) was applied and incubated for 1 h at 37 °C. Then, anti-mouse IgG conjugated to alkaline phosphatase (1:4000; Sigma–Aldrich), followed by *p*-nitrophenylphosphate (Bio-Rad Laboratories Inc., Redmond, WA, USA) was added and incubated at 37 °C for 20 min. The optical density at 415 nm (OD_{415}) was measured with a microplate reader (Bio-Rad).

2.4. Immunization of mice

Seven-week-old female BALB/c mice (Japan SLC, Shizuoka, Japan), with 12–21 mice per group, were subcutaneously (s.c.) injected three times with D3 alone, a mixture of D3 and COMP–Z, the COMP–Z/D3 tricomponent complex (chemical conjugation), D3–COMP–Z or Z–COMP–D3 (genetic fusion) at weeks 0, 2,

Table 1
Oligonucleotides used in this study.

Oligonucleotide number	Nucleotide sequence
#1	5′-CATGGGTCCGGGCCCGGGTGGCGGTGGCAGCCACCATCACCATCACCACGGTGGCGGTGGCAGCGGTCCGGGCCCGGG-3′
#2	5′-CATGCCCGGGCCCGGACCGCTGCCACCGCCACCGTGGTGATGGTGATGGTGGCTGCCACCGCCACCCGGGCCCGGACC-3′
#3	5′-CGCCCATGGACAAACTGGCTCTGAAAGGCACA-3′
#4	5′-GCGCCATGGCCGTGCTTCCAGCCTTGTACCA-3′
#5	5′-CGCCTCGAGGACAAACTGGCTCTGAAAGGCACA-3′
#6	5′-GCGCTCGAGTTACGTGCTTCCAGCCTTGTACCA-3′
#7	5′-GCGCTCGAGGTGGATAACAAATTTAATAAAGAACAGC-3′
#8	5′-GCGCTCGAGTTATTTCGGGGCCTGTGCATCG-3′
#9	5′-GCGCCATGGTGGATAACAAATTTAATAAAGAACAG-3′
#10	5′-GCGCCATGGCTTTCGGGGCCTGTGCATCG-3′

The underlined sequences indicate restriction enzyme recognition sites.

and 4. Aluminum hydroxide (Imject Alum Adjuvant, Thermo Scientific, Inc.) was used as the adjuvant. For tricomponent complexes generated by genetic fusion, either unfractionated protein, high-molecular-mass fraction, or pentamer fraction was used as immunization material. All immunization samples contained equivalent amounts of D3 (30 μg). The amount of D3 protein moiety contained in the tricomponent complexes was calculated based on the molecular mass ratio between the D3 protein moiety and the whole fusion protein. The amount of total protein contents in the immunization samples was measured by BCA assay. As a positive control, a mouse-brain-derived formalin-inactivated JE vaccine (strain Beijing-1; Chemo-Sero-Therapeutic Research Institute, Kumamoto, Japan) was administered twice intraperitoneally (i.p.) to 7-week-old female BALB/c mice in a volume of 100 μl with 3-day interval at week 4, according to the manufacturer's protocol. Blood samples were collected at week 6 from the tail vein for the virus neutralization test.

Animal experimental protocols were approved by the Institutional Animal Care and Use Committee (the internal ethics registration number: 4995) and animal experiments were conducted according to the institutional ethical guidelines for animal experiments.

2.5. Virus neutralization test

A virus-neutralizing antibody assay was conducted as described previously with a 50% focus reduction neutralization test ($FRNT_{50}$) [7]. Briefly, 10 μl of virus solution was mixed with 10 μl of serially diluted heat-inactivated antiserum. The mixture was incubated at 28 °C for 2 h and then added to BHK-21 cell monolayers. The plates were incubated further at 37 °C for 2 h under 5% CO_2. After incubation, 80 μl of medium containing 0.8% methylcellulose (Wako Pure Chemical Industries, Osaka, Japan) was added and incubated in a CO_2 incubator at 37 °C for 24 h. The cells were fixed with methanol, and incubated with rabbit anti-JE antiserum and goat anti-rabbit horseradish-peroxidase-conjugated IgG (Cappel Laboratories, Inc., Cochranville, PA, USA). The color reaction was developed with 0.01% H_2O_2 and 3–3′-diaminobenzidine tetrahydrochloride (Wako) in PBS.

2.6. Viral challenge

The JEV infection experiments were conducted as described previously [7]. Briefly, 2 weeks after the last immunization (at week 6), the mice were challenged i.p. with 1×10^5 focus-forming units (FFU) of JEV strain JaGAr01 (50 LD_{50}) immediately after an intracerebral (i.c.) injection of 50 μl of PBS. The mice were monitored daily until day 28 after infection for behavioral and physical symptoms, such as paralysis, and their survival data were recorded.

2.7. Statistical analysis

Statistically significant differences were determined with the Wilcoxon–Mann–Whitney test for the virus-neutralizing antibody titers. The Kaplan–Meier log-rank test was used to compare the survival curves of the control group and a specified immunization group, or two specific immunization groups. Statistical analyses were conducted with JMP software version 8.0 (SAS Institute Inc., Cary, NC, USA).

3. Results and discussion

Many safe and potent vaccines include live attenuated and killed pathogens, but it may be preferable in some cases to mount immune responses against specific antigens or epitopes derived from the target pathogens, rather than to mount broad responses to large repertoires of structural units of the pathogenic organisms. In these cases, subunit vaccines consisting of specific antigens, designed and produced by recombinant DNA technology, provide formidable advantages. However, highly purified innocuous protein antigens require adjuvants to induce sufficient levels of immunity for protection against lethal pathogenic infections.

The adjuvants most widely used with robust safety are aluminum salts. Nevertheless, recent human clinical trials (for example, in malaria vaccine development [8]) have indicated that alum adjuvants are often insufficiently strong to induce an antibody response to recombinant-protein-based subunit vaccines. Therefore, the development of stronger and safe adjuvants is urgently required. It is also true that stronger adjuvants are more likely to induce stronger reactogenicity, so the development of novel adjuvants represents a formidable challenge. Soluble innocuous proteins alone are very weakly immunogenic, first because they do not contain pathogen-associated molecular patterns (PAMPs) that can elicit an innate immune response, which are prerequisites for the efficient induction of adaptive immunity [9]. Second, antigens that do not represent particulate structures are weak inducers of B-cell activation [10]. Third, antigens that are not efficiently taken up by professional APCs are likely to be cleared from the system without eliciting strong adaptive immunity [2]. Therefore, increasing the protein mass by forming multimers [11] or particulate structures is a promising and practically feasible way to transform innocuous recombinant proteins into potent subunit vaccines [12]. For this reason, we have recently developed a novel vaccine platform technology, designated the "tricomponent immunopotentiating system" (TIPS) [4], to meet all the important criteria required for the creation of effective recombinant vaccines. To evaluate the immunogenic efficacy of TIPS, we first demonstrated that the COMP–Z fusion complex loaded with the *Plasmodium vivax* ookinete surface protein, Pvs25, a transmission-blocking candidate vaccine for *P. vivax* malaria, or the C-terminal 19-kDa fragment of *P. yoelii* merozoite surface protein-1 (MSP1-19), an antigen expressed

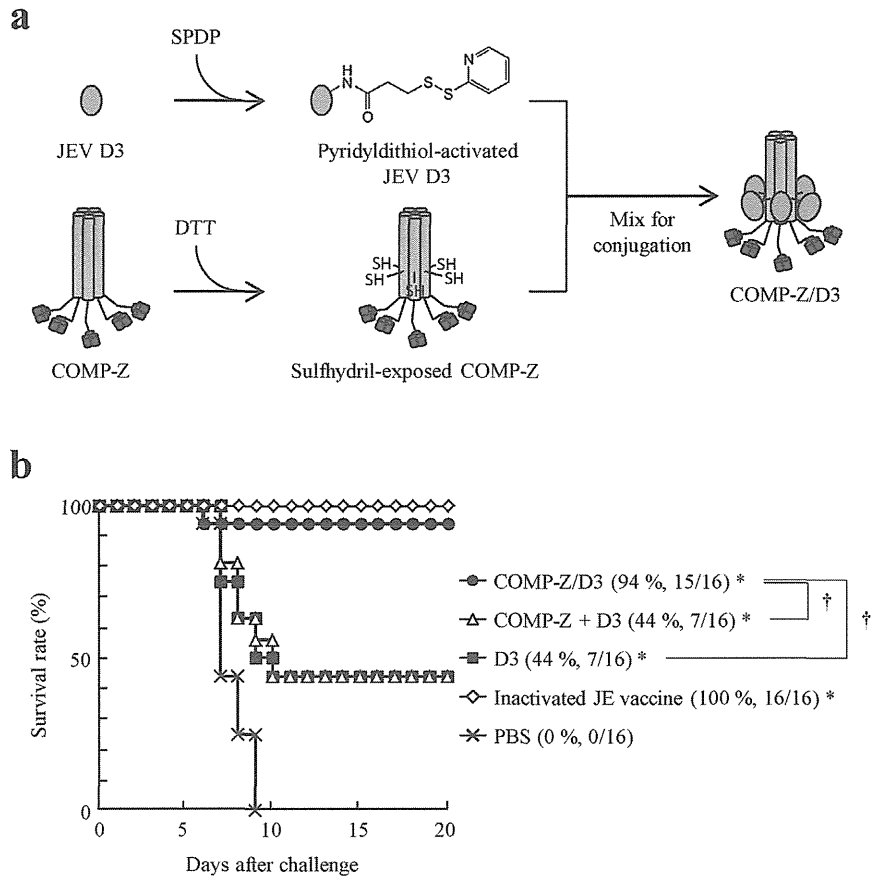

Fig. 1. Generation of the chemically conjugated COMP–Z/D3 tricomponent complex and its protective efficacy against a lethal Japanese encephalitis virus (JEV) infection in mice. (a) *Escherichia coli*-expressed recombinant D3 protein was treated with the heterobifunctional cross-linking reagent *N*-succinimidyl 3-(2-pyridyldithio) propionate (SPDP) to modify its primary amines. Simultaneously, the *E. coli*-expressed COMP–Z delivery molecule [4] was treated with dithiothreitol (DTT) to generate free sulfhydryl groups at the cysteine residues located near the C-terminal region of the COMP coiled-coil motif. These two proteins were mixed for conjugation to generate the COMP–Z/D3 tricomponent complex. (b) The protective efficacy of the COMP–Z/D3 tricomponent complex against a lethal JEV infection was evaluated. Seven-week-old female BALB/c mice (16 mice per group) were subcutaneously injected three times with D3 alone, a mixture of D3 and COMP–Z, or the COMP–Z/D3 tricomponent complex at weeks 0, 2, and 4. Aluminum hydroxide was used as the adjuvant. Two weeks after the third immunization, the mice were challenged with 1×10^5 FFU of JEV strain JaGAr01 (50 LD_{50}) via an intraperitoneal (i.p.) route. To increase the cerebral infectivity of the virus, 50 μl of PBS was injected intracerebrally immediately before the i.p. viral challenge. The mice were monitored for 3 weeks after infection for signs of behavioral or physical abnormalities and their survival rates were recorded. Survival rates are expressed in percentages; the numbers of surviving mice per total number of challenged mice are given in parentheses. D3, unloaded D3 protein; COMP–Z + D3, a mixture of COMP–Z and D3. *$P < 0.01$ vs. PBS group; †$P < 0.01$ between the two indicated groups analyzed with the log-rank test.

in the asexual stage of a rodent malarial parasite, induced robust antiparasite immunity [4].

In the present study, we selected a mouse JEV infection model for a proof-of-concept evaluation of the TIPS platform technology to determine whether it can be applied to the development of vaccines for viral infections. We previously demonstrated that the JEV E protein expressed in *E. coli* confers potent protection against lethal JEV infection in mice [7]. In the present study, we selected the JEV E protein D3, which constitutes the C-terminal one-third of the E protein, because this domain was more stable as a water-soluble form and is more efficiently produced when expressed in *E. coli* than the full-length E protein. Therefore, it confers a formidable advantage when it is manipulated to create the chemical or genetic fusion complex.

To load D3 onto COMP–Z, the protein was first treated with the heterobifunctional cross-linker SPDP to generate pyridildithiol-activated D3, and was then mixed with DTT-treated COMP–Z for conjugation (Fig. 1a). Because the COMP coiled-coil domain contains cysteine residues, the reduced sulfhydryls reacted with the pyridildithiol-activated D3 to generate the tricomponent complex COMP–Z/D3. The generated complex retained its immunoglobulin-binding domain (IBD) function, confirmed by human IgG ELISA (data not shown). Next, BALB/c mice were immunized s.c. with the COMP–Z/D3 complex, and the animals were subjected to lethal infection with JEV. In our mouse JEV infection protocol, the i.p. administration of 1×10^5 FFU (50 LD_{50}), followed by an i.c. injection of PBS, consistently killed 100% of naïve mice or PBS (mock)-administered mice within 1–2 weeks after infection, whereas i.p. immunization with a formalin-inactivated JE vaccine provided complete protection [7]. We demonstrated that immunization with the COMP–Z/D3 complex conferred 94% protection (15/16) (Fig. 1b). On the contrary, immunization with D3 alone or D3 not integrated into the tricomponent complex (i.e., a mixture of D3 and COMP–Z) conferred only 44% protection (7/16) (Fig. 1b). This seminal study indicated that loading a viral antigen onto the COMP–Z delivery vehicle robustly augmented immunogenicity of the antigen, a result consistent with our previous observation of malaria parasite antigens [4].

Genetic fusion is generally considered superior to chemical conjugation for the generation of homogeneous molecules. However, malaria parasite antigens, such as Pvs25, composed of a series of epidermal-growth-factor-like domains, are difficult to produce in *E. coli* as recombinant antigens that retain their native folds. Therefore, we previously had no choice but to use chemical conjugation to load the parasite antigens onto COMP–Z [4]. In contrast, given that both D3 and COMP–Z could be expressed in *E. coli* at

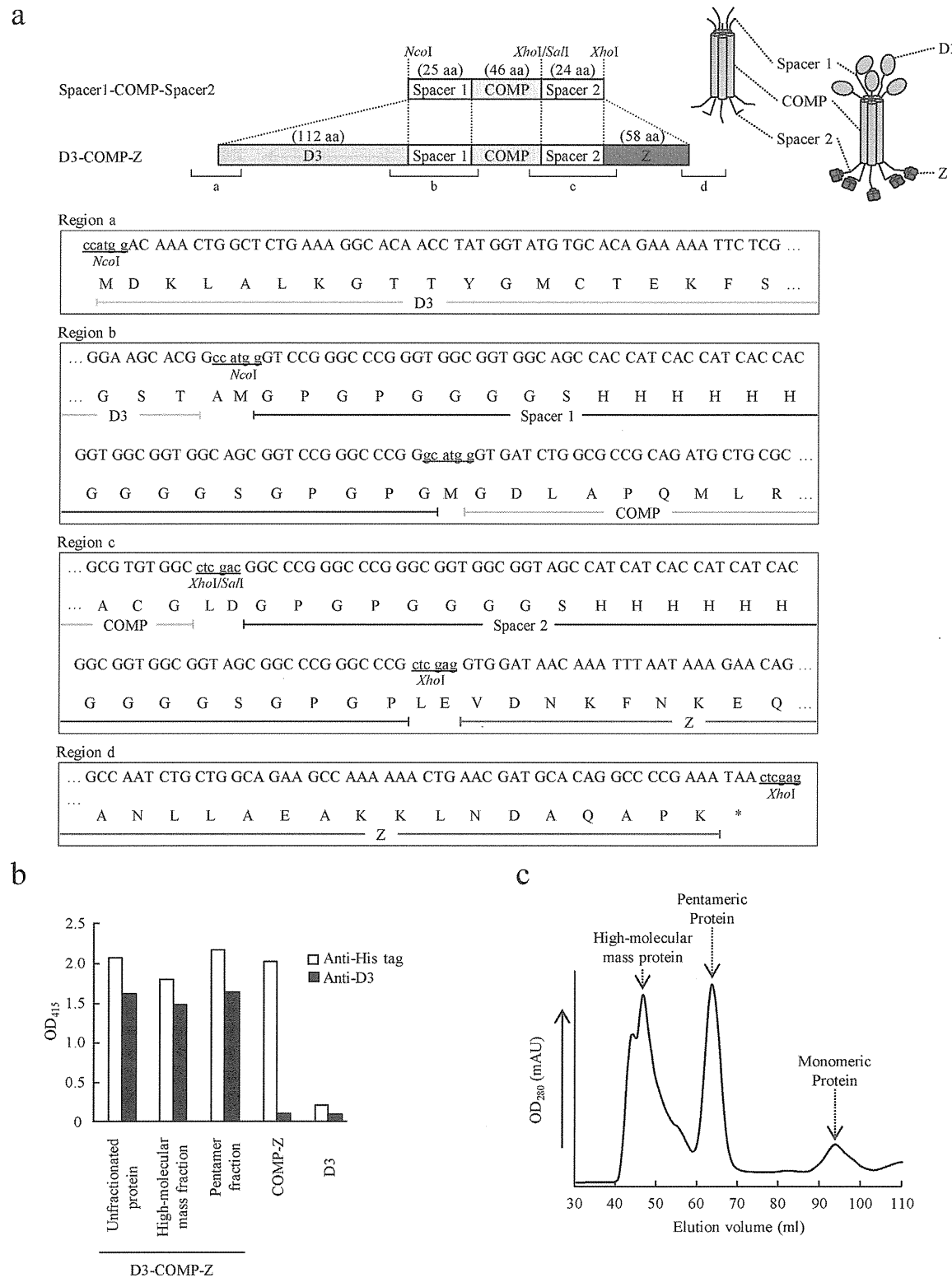

Fig. 2. Generation of the genetically conjugated D3–COMP–Z tricomponent complex. (a) A schematic drawing of the D3–COMP–Z tricomponent genetic fusion complex: Spacer1–COMP–Spacer2, the COMP coiled-coil domain (46 amino acids of $COMP_{27-72}$) containing the N- and C-terminal spacer sequences (designated "Spacer 1" and "Spacer 2", respectively); D3–COMP–Z, Spacer1–COMP–Spacer2 fused to the D3 coding sequence at the N-terminus and the Z-domain coding sequence at the C-terminus. Regions a–d indicate the nucleotide and amino acid sequences of the corresponding regions of the fusion complex. The Spacer1–COMP–Spacer2 sequence was inserted between the *Nco*I and *Xho*I sites of the pET-21d vector. The D3 protein and Z-domain coding regions were inserted at the *Nco*I and *Xho*I sites, respectively, of the pET-21d–Spacer1–COMP–Spacer2 expression plasmid. (b) Unfractionated and fractionated proteins were analyzed with a human IgG ELISA using anti-His tag (open bars) or anti-D3 (filled bars) antiserum to confirm the integrity of the tricomponent complex. (c) The D3–COMP–Z fusion protein was fractionated by size-exclusion chromatography to separate the pentamers from the high-molecular-mass protein species for the immunization study.

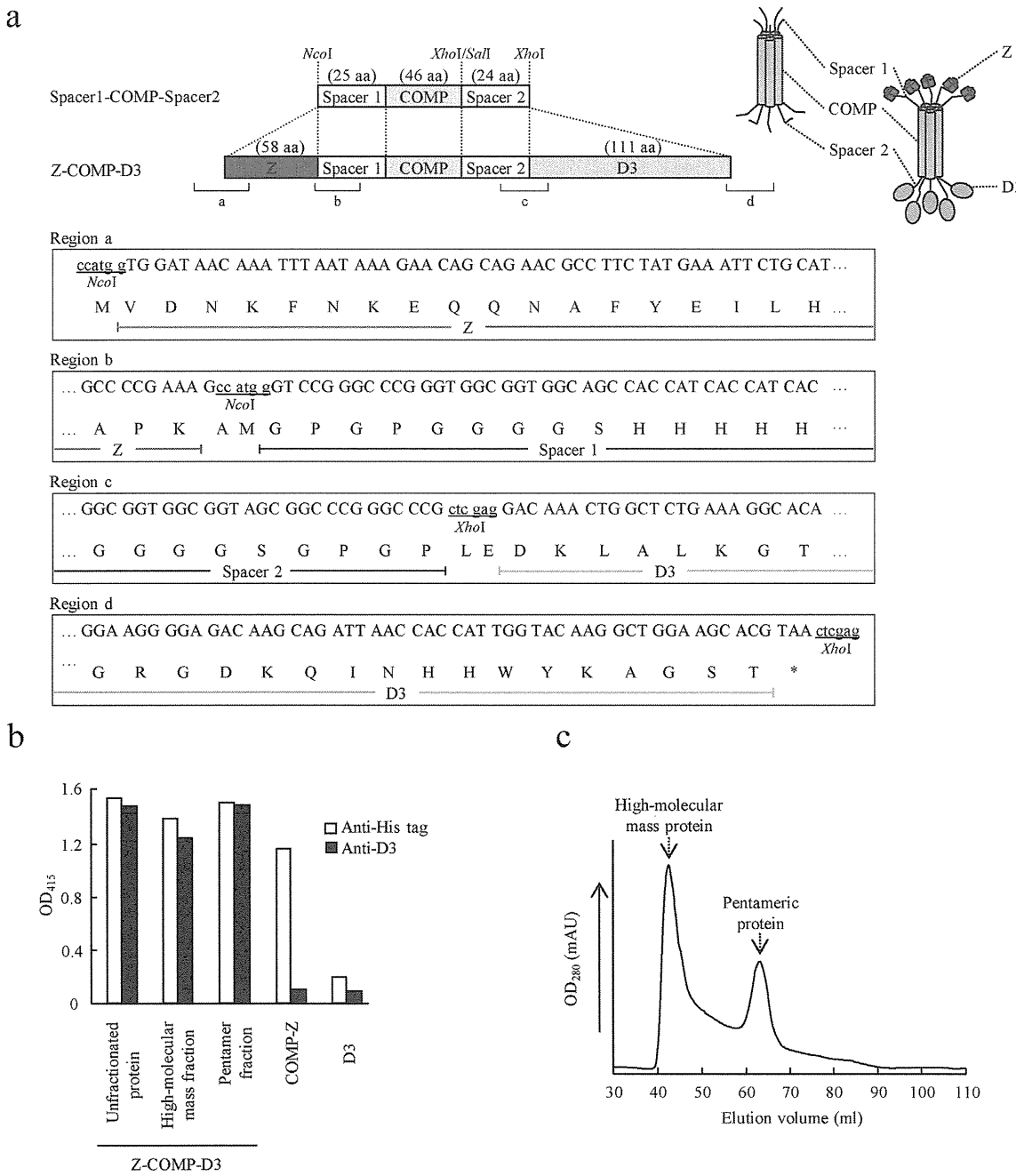

Fig. 3. Generation of the genetically conjugated Z–COMP–D3 tricomponent complex. (a) A schematic drawing of the Z–COMP–D3 tricomponent genetic fusion complex: Spacer1–COMP–Spacer2, see legend of Fig. 2a; Z–COMP–D3, the Spacer1–COMP–Spacer2 fused to the Z-domain coding sequence at the N-terminus and the D3 coding sequence at the C-terminus. Regions a–d indicate the nucleotide and amino acid sequences of the corresponding regions of the fusion complex. The Z domain and D3 protein coding regions were inserted at the *Nco*I and *Xho*I sites, respectively, of the pET-21d–Spacer1–COMP–Spacer2 expression plasmid. (b) Unfractionated and fractionated proteins were analyzed with a human IgG ELISA using anti-His tag (open bars) or anti-D3 (filled bars) antiserum to confirm the integrity of the tricomponent complex. (c) The Z–COMP–D3 fusion protein was fractionated by size-exclusion chromatography to separate the pentamers from the high-molecular-mass protein species for the immunization study.

substantial levels, retaining their biological functions, we investigated whether genetic conjugation was feasible for generating the tricomponent complex. To this end, we constructed two types of tricomponent complex, in which the positions of D3 and Z were switched: D3–COMP–Z and Z–COMP–D3 (Figs. 2a and 3a). These fusion proteins were produced in *E. coli* as inclusion bodies, but upon solubilization with 8 M urea followed by dialysis against PBS, they refolded to regain their D3 antigenicity and IBD functions (Figs. 2b and 3b; Supplemental Figs. 1a and b), which indicated that the Z domain was also refolded to its native configuration by the refolding process. Size-exclusion chromatography revealed that both pentameric and high-molecular-mass protein species were produced (Figs. 2c and 3c). We observed only homogeneous pentamers of the antigen-unloaded COMP–Z [4] and a tricomponent complex in which a short protein epitope of only 25 amino acids derived from human T-cell leukemia virus 1 was genetically fused to COMP–Z, but no high-molecular-mass protein species were detected (unpublished data). These results suggest that the D3 protein moiety of the tricomponent complex, which might not have completely refolded to its native conformation, has a tendency to aggregate, and functions as an aggregation core to generate high-molecular-mass molecules. An additional advantage of genetically

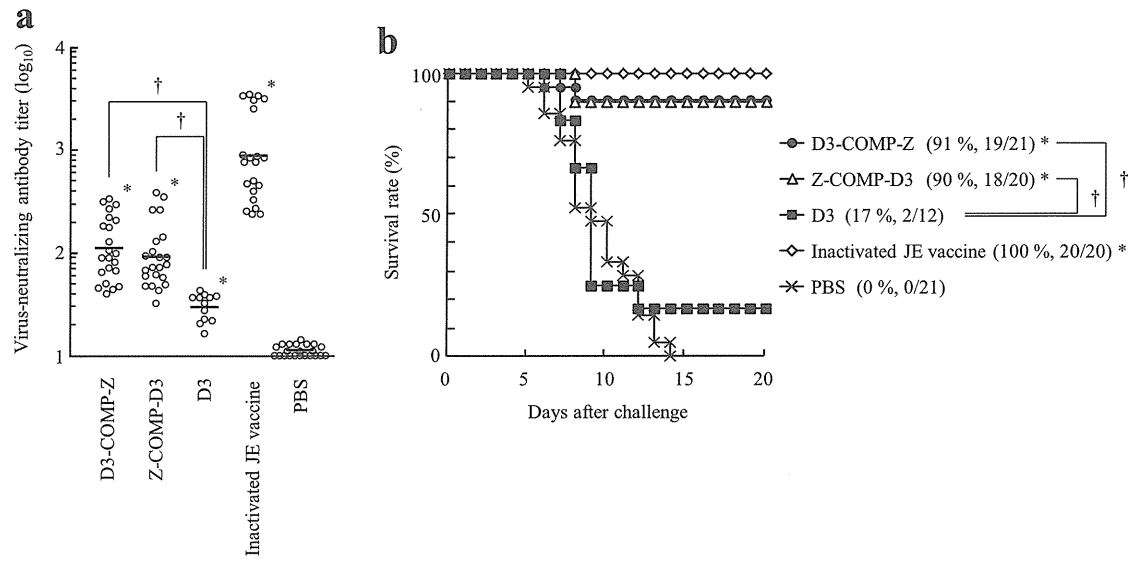

Fig. 4. Vaccine efficacies of the pentameric D3–COMP–Z and Z–COMP–D3 tricomponent complexes. (a) JEV-neutralizing antibody titers for the antisera collected at week 6. Female BALB/c mice were immunized with the pentameric D3–COMP–Z or Z–COMP–D3 fusion complex (fractions 60–70 mL collected by size-exclusion chromatography presented in Fig. 2c or 3c, respectively), each dose of which was calculated to include 30 μg of the D3 protein moiety. The immunization schedule and infection protocol were identical to those described in the legend of Fig. 1b. $^{*}P < 0.01$ vs. PBS group; $^{\dagger}P < 0.01$ between the two indicated groups analyzed with the Wilcoxon–Mann–Whitney test. (b) Protective efficacy of the tricomponent complexes against a lethal JEV infection, as described in the legend of Fig. 1b. Survival rates are expressed in percentages; the numbers of surviving mice per total number of infected mice are also provided in parentheses. $^{*}P < 0.01$ vs. PBS group; $^{\dagger}P < 0.01$ between the two indicated groups analyzed with the log-rank test.

fusing D3 to COMP–Z is that its water solubility is significantly improved compared with that of the D3 protein alone. The D3 protein showed a tendency to form insoluble aggregates upon repeated freeze-and-thaw processes, whereas both D3–COMP–Z and Z–COMP–D3 did not. This is a considerable advantage in vaccine manufacture, and this biochemical characteristic is probably attributable to the high water solubility of the COMP–Z molecule.

Supplementary material related to this article can be found, in the online version, at http://dx.doi.org/10.1016/j.vaccine.2013.12.016.

The final protein yield for the PBS-exchanged D3–COMP–Z and Z–COMP–D3 was 50 mg/L and 100 mg/L of bacterial culture, respectively, for unfractionated whole protein, 30 mg/L and 16 mg/L for the high-molecular-mass protein species, respectively, and 12 mg/L and 48 mg/L for the pentamer species, respectively.

We have previously demonstrated that all three constituent components of TIPS are essential to induce effective immune responses [4]. To confirm that this is also true for the D3-based JE vaccine model, we attempted to create fusion proteins lacking the Z domain. However, after solubilization in 8 M urea, the D3–COMP and COMP–D3 fusion proteins were subjected to a refolding process by dialysis against PBS, and they immediately formed aggregations. This was not observed for the D3 protein alone, so we presumed that the multimerization of D3 by the pentameric COMP coiled-coil domain significantly facilitated the aggregation process. Therefore, we concluded that the Z domain is essential for antigen delivery [4], and that in some cases, the Z domain is essential to improve the water solubility of the complex to avoid the formation of insoluble aggregates.

Finally, we immunized mice with the pentameric tricomponent complexes, which had been separated from high-molecular-mass protein species by size-exclusion chromatography. Immunization materials used for this experiment were fractions 60–70 mL collected by size-exclusion chromatography (Figs. 2c and 3c), and the materials contained alum adjuvant. As shown in Fig. 4a, immunization with the pentameric D3–COMP–Z or Z–COMP–D3 tricomponent complex induced significantly elevated JEV-neutralizing antibodies compared with unloaded D3 protein. Furthermore, when the immunized mice were challenged with a lethal dose of JEV, approximately 90% of the animals survived (Fig. 4b). In contrast, unloaded D3 conferred only 17% protection (Fig. 4b), indicating that the integration of the antigen into the tricomponent complex robustly augmented its protective efficacy against viral infection. This result is consistent with the data presented in Fig. 1. We also tested the vaccine efficacy of unfractionated tricomponent complexes as well as high-molecular-mass protein species (fractions 40–50 mL in Figs. 2c and 3c) mixed with alum adjuvant. Immunization with unfractionated whole protein conferred comparable levels of protection, i.e., 91% for D3–COMP–Z and 84% for Z–COMP–D3 (Table 2). Immunization with the high-molecular mass protein species also showed almost comparable levels of protection (Table 2). Immunization with the tricomponent complexes not containing alum adjuvant generally conferred 20–40% lower protection levels (data not shown), confirming that protein multimerization, APC-targeting, and innate immunity induction properties of vaccine formulations are necessary to be combined for the better vaccine efficacy. The unfractionated proteins contained high-molecular-mass protein species, which were soluble aggregates of the complex. As mentioned above, the soluble aggregates might have been generated by incompletely folded D3 protein, which functioned as a

Table 2
JEV challenge experiments conducted by using unfractionated whole protein or high-molecular-mass fraction of the tricomponent complexes mixed with alum adjuvant.

Immunization material	Unfractionated whole protein	High-molecular mass fraction
D3–COMP–Z	20/22 (91%)	8/9 (88.8%)
Z–COMP–D3	16/19 (84%)	6/8 (75.0%)
Inactivated JE vaccine	20/20 (100%)	10/10 (100%)
PBS	0/21 (0%)	0/9 (0%)

Data are expressed as the number of survived mice per total number of mice infected with a lethal dose of JEV (50 LD_{50}).

hydrophobic aggregation core. It is assumed that incompletely folded proteins less efficiently provide the native protective epitopes recognized by B lymphocytes. However, high-molecular-mass proteins show a tendency to induce higher antibody responses than low-molecular-mass proteins containing the same epitopes [10]. Therefore, these conflicting effects might have offset one another to maintain the level of protective immunity against viral infection.

In this study, we created two types of a genetically fused complex, D3–COMP–Z and Z–COMP–D3, in which the only difference was the relative positions of D3 and Z. Both constructs showed similar D3 antigenicity and IBD functions (Figs. 2b and 3b), chromatographic profiles (Figs. 2c and 3c), immunogenicity (Fig. 4a), and vaccine efficacy (Fig. 4b). These results indicate that the Z domain can function as the IBD when placed at either the N- or C-terminus of the COMP coiled-coil moiety. This was also true for the D3 antigen. However, depending on the vaccine proteins to be fused, masking the N- or C-terminus may negatively affect the protein folding, consequently affecting the efficacy of the vaccine. If this is the case for a given protein of interest, then either the COMP–Z or Z–COMP can be chosen as the better fusion partner.

Protection against lethal JEV infection is primarily mediated by neutralizing antibodies. Therefore, molecular design optimized to induce virus particle-specific antibodies with virus-neutralizing capacity is paramount importance for creating effective JE vaccines. Fig. 4a shows that virus-neutralizing antibody titers attained by the complexes are significantly higher than 10. In the $FRNT_{50}$, antibody titers above 10–20 are considered seropositive and could potentially provide protection against the lethal virus infection. Immunization with the D3 protein with alum adjuvant conferred only 17% of protection, but the tricomponent complexes were 90% protective (Fig. 4b). This difference in protective efficacy could be explained by the difference in virus-neutralizing antibody titers, which were significantly different between these two vaccine materials (titers: 30 vs. 100). For the inactivated JE vaccine the virus-neutralizing antibody titer approached 1000, which was high enough to provide complete protection against the lethal virus infection (Fig. 4b). Although titers for the tricomponent complexes were much lower than the titer attained by the JE vaccine, we reasoned that titers around 100 provide high levels of protection against the lethal virus infection.

Although commercial JE vaccines exist, there have been several promising attempts to create next-generation JE vaccines. For example, Alka et al. [13] reported that D3 protein produced in *E. coli* as a His-tag or maltose-binding-protein fusion protein conferred approximately 80% protection against lethal JEV challenge infection when administered to mice with an aluminum hydroxide adjuvant. Wu et al. [14] reported that immunization with a D3–thioredoxin fusion protein with incomplete Freund's adjuvant or cationic liposomes conferred 60% or 80% protection in mice, respectively. Verma et al. [15] reported that immunization with D3 with Freund's adjuvant induced high levels of virus-neutralizing antibodies in mice. The inclusion of oil-based adjuvants is effective in immunization regimes for D3-based vaccines, although many of them are unsuitable for human use because of their potentially high reactogenicity. In contrast, aluminum-salt-based adjuvants have a long history of safe use in humans, but are often not strong enough to induce protective immunity when used with recombinant proteins. Therefore, a combination of protein delivery systems and aluminum salt adjuvants may provide a promising solution to the provision of strong protective immunity by recombinant-protein-based vaccines.

In this study, we exploited an antigen-delivery molecule including the COMP coiled-coil domain and a B-lymphocyte targeting ligand to enhance the immunogenicity of the recombinant JEV E protein antigen, which is otherwise very weakly immunogenic. Our results clearly demonstrate that the JEV D3 antigen loaded onto the delivery molecule robustly augmented the antiviral immunity in a mouse model of JEV infection. The tricomponent complex is an efficient inducer of humoral immunity against the protein antigens loaded, as demonstrated in the present study of JEV infection and previously in models of malaria infection [4]. Therefore, it is reasonable to expect that there are other infections that could be effectively controlled by this vaccine platform technology, particularly those that are primarily controlled by antibodies. Further studies are underway to evaluate the versatility of the tricomponent complex for the design of subunit vaccines for infectious diseases.

Acknowledgements

This work was supported by the Program for the Promotion of Basic Research Activities for Innovative Biosciences from the Bio-oriented Technology Research Advancement Institution in Japan, and a Cooperative Research Grant from the Institute of Tropical Medicine, Nagasaki University, Japan.

References

[1] Banchereau J, Steinman RM. Dendritic cells and the control of immunity. Nature 1998;392:245–52.
[2] Caminschi I, Shortman K. Boosting antibody responses by targeting antigens to dendritic cells. Trends in Immunology 2012;33:71–7.
[3] Tacken PJ, Torensma R, Figdor CG. Targeting antigens to dendritic cells in vivo. Immunobiology 2006;211:599–608.
[4] Miyata T, Harakuni T, Tsuboi T, Sattabongkot J, Ikehara A, Tachibana M, et al. Tricomponent immunopotentiating system as a novel molecular design strategy for malaria vaccine development. Infection and Immunity 2011;79:4260–75.
[5] Efimov VP, Lustig A, Engel J. The thrombospondin-like chains of cartilage oligomeric matrix protein are assembled by a five-stranded alpha-helical bundle between residues 20 and 83. FEBS Letters 1994;341:54–8.
[6] Tashiro M, Tejero R, Zimmerman DE, Celda B, Nilsson B, Montelione GT. High-resolution solution NMR structure of the Z domain of staphylococcal protein A. Journal of Molecular Biology 1997;272:573–90.
[7] Tafuku S, Miyata T, Tadano M, Mitsumata R, Kawakami H, Harakuni T, et al. Japanese encephalitis virus structural and nonstructural proteins expressed in *Escherichia coli* induce protective immunity in mice. Microbes and Infection/Institut Pasteur 2012;14:169–76.
[8] Malkin EM, Durbin AP, Diemert DJ, Sattabongkot J, Wu Y, Miura K, et al. Phase 1 vaccine trial of Pvs25H: a transmission blocking vaccine for *Plasmodium vivax* malaria. Vaccine 2005;23:3131–8.
[9] Akira S. Innate immunity and adjuvants. Philosophical Transactions of the Royal Society of London Series B, Biological Sciences 2011;366:2748–55.
[10] Link A, Zabel F, Schnetzler Y, Titz A, Brombacher F, Bachmann MF. Innate immunity mediates follicular transport of particulate but not soluble protein antigen. Journal of Immunology (Baltimore, MD: 1950) 2012;188:3724–33.
[11] Wibowo N, Chuan YP, Lua LHL, Middelberg APJ. Modular engineering of a microbially-produced viral capsomere vaccine for influenza. Chemical Engineering Science 2013;103:12–20.
[12] Arakawa T. Adjuvants: no longer a 'dirty little secret', but essential key players in vaccines of the future. Expert Review of Vaccines 2011;10:1–5.
[13] Alka, Bharati K, Malik YP, Vrati S. Immunogenicity and protective efficacy of the *E. coli*-expressed domain III of Japanese encephalitis virus envelope protein in mice. Medical Microbiology and Immunology 2007;196:227–31.
[14] Wu SC, Yu CH, Lin CW, Chu IM. The domain III fragment of Japanese encephalitis virus envelope protein: mouse immunogenicity and liposome adjuvanticity. Vaccine 2003;21:2516–22.
[15] Verma SK, Gupta N, Pattnaik P, Babu JP, Rao PV, Kumar S. Antibodies against refolded recombinant envelope protein (domain III) of Japanese encephalitis virus inhibit the JEV infection to porcine stable kidney cells. Protein and Peptide Letters 2009;16:1334–41.

PLOS ONE

Structure and Dynamics of the gp120 V3 Loop That Confers Noncompetitive Resistance in R5 HIV-1_{JR-FL} to Maraviroc

Yuzhe Yuan[1], Masaru Yokoyama[2], Yosuke Maeda[3], Hiromi Terasawa[3], Shinji Harada[3], Hironori Sato[2], Keisuke Yusa[4]*

1 Transfusion Transmitted Diseases Center, Institute of Blood Transfusion, Chinese Academy of Medical Science, Chenghua District, Chengdu, Sichuan Province, P. R. China, **2** Pathogen Genomics Center, National Institute of Infectious Diseases, Musashi Murayama, Tokyo, Japan, **3** Department of Medical Virology, Graduate School of Medical Sciences, Kumamoto University, Kumamoto, Japan, **4** Division of Biological Chemistry and Biologicals, National Institute of Health Sciences, Setagaya, Tokyo, Japan

Abstract

Maraviroc, an (HIV-1) entry inhibitor, binds to CCR5 and efficiently prevents R5 human immunodeficiency virus type 1 (HIV-1) from using CCR5 as a coreceptor for entry into $CD4^+$ cells. However, HIV-1 can elude maraviroc by using the drug-bound form of CCR5 as a coreceptor. This property is known as noncompetitive resistance. HIV-$1_{V3\text{-}M5}$ derived from HIV-$1_{JR\text{-}FLan}$ is a noncompetitive-resistant virus that contains five mutations (I304V/F312W/T314A/E317D/I318V) in the gp120 V3 loop alone. To obtain genetic and structural insights into maraviroc resistance in HIV-1, we performed here mutagenesis and computer-assisted structural study. A series of site-directed mutagenesis experiments demonstrated that combinations of V3 mutations are required for HIV-$1_{JR\text{-}FLan}$ to replicate in the presence of 1 μM maraviroc, and that a T199K mutation in the C2 region increases viral fitness in combination with V3 mutations. Molecular dynamic (MD) simulations of the gp120 outer domain V3 loop with or without the five mutations showed that the V3 mutations induced (i) changes in V3 configuration on the gp120 outer domain, (ii) reduction of an anti-parallel β-sheet in the V3 stem region, (iii) reduction in fluctuations of the V3 tip and stem regions, and (iv) a shift of the fluctuation site at the V3 base region. These results suggest that the HIV-1 gp120 V3 mutations that confer maraviroc resistance alter structure and dynamics of the V3 loop on the gp120 outer domain, and enable interactions between gp120 and the drug-bound form of CCR5.

Citation: Yuan Y, Yokoyama M, Maeda Y, Terasawa H, Harada S, et al. (2013) Structure and Dynamics of the gp120 V3 Loop That Confers Noncompetitive Resistance in R5 HIV-$1_{JR\text{-}FL}$ to Maraviroc. PLoS ONE 8(6): e65115. doi:10.1371/journal.pone.0065115

Editor: Jean-Pierre Vartanian, Institut Pasteur, France

Received February 14, 2013; **Accepted** April 21, 2013; **Published** June 28, 2013

Funding: This work was supported by grants from the Ministry of Health, Labour and Welfare and by the Global COE program Education and Research Center Aiming at the Control of AIDS from the Ministry of Education, Science, Sports and Culture, Japan. Y.Y. was supported by National Natural Science Foundation of China (81201329), scholarship for youth from Chinese Academy of Medical Sciences and Peking Union Medical College. The funders had no role in study design, data collection and analysis, decision to publish, or preparation of the manuscript.

Competing Interests: The authors have declared that no competing interests exist.

* E-mail: yusak@nihs.go.jp

Introduction

Inhibiting the entry of R5 human immunodeficiency virus type 1 (HIV-1) into $CCR5^+/CD4^+$ cells is an effective step in blocking viral replication. An entry inhibitor can bind to CCR5 and prevent R5 HIV-1 from using CCR5 as a coreceptor for entry [1]. Maraviroc, a CCR5 antagonist, has potent *in vitro* and *in vivo* antiviral activity against laboratory strains and clinical isolates [2–4]. Maraviroc, approved in 2007, was the first CCR5 antagonist approved by the US Food and Drug Administration and is currently used to treat patients with R5-tropic HIV-1 infections.

Treatment failures can occur because of an increasing number of pre-existing CXCR4-using viruses [5,6]. Alternatively, escape mutants can evade a CCR5 inhibitor by accumulating multiple mutations in gp120 and/or gp41 without switching their coreceptor usage [7–14]. Escape mutants can use the drug-bound form of CCR5 as a coreceptor, a property known as noncompetitive resistance [8,9,11]. In noncompetitive-resistant viruses, drug-free CCR5 usage is compatible with the additional ability of drug-bound CCR5 usage. We previously reported that a combination of polymorphic mutations in the gp120 V3 loop can confer noncompetitive resistance in HIV-$1_{JR\text{-}FL}$ [15]. One of these viruses, designated HIV-$1_{V3\text{-}M5}$, contains a set of five mutations I304V/F312W/T314A/E317D/I318V in the V3 loop (from Cys^{293} to Cys^{327}). Most other noncompetitive-resistant viruses contain multiple mutations in the V3 loop [8,9,11], although mutations reported till date in the V3 loop are not always common and resistance-associated mutations in the V3 loop were considered to be background dependent. Two elements are involved in gp120 coreceptor binding: (i) the V3 tip for the CCR5 extracellular loop 2 (ECL2) and (ii) the V3 base and stem residues and the V3 base of the gp120 core for the CCR5 N terminus [16–19]. Thus, the V3 loop of HIV-1 plays a pivotal role in its interaction with CCR5. However, how the V3 mutations induce maraviroc-resistance without changing coreceptor tropism remains unknown.

Increasing evidence indicates that the protein surface fluctuates in solution, and that such fluctuations play key roles in interactions with other molecules [20][20,23]. We previously suggested that the structural dynamics of the HIV-1 gp120 V3 loop play key roles